

Optimization, kinetics, equilibrium isotherms, and thermodynamics studies of Coomassie violet dye adsorption using *Azadirachta indica* (neem) leaf adsorbent

J.M. Divya, K. Palak, P. Vairavel*

Department of Chemical Engineering, Manipal Institute of Technology, Manipal Academy of Higher Education (MAHE), Manipal, Karnataka State, India, Tel. +91 9036270978; email: pvairavel@gmail.com (P. Vairavel), Tel. +91 8073099491; email: joslin.mathias95@gmail.com (J.M. Divya), Tel. +91 7259631036; email: kaurpalak3@gmail.com (K. Palak)

Received 11 August 2019; Accepted 14 February 2020

ABSTRACT

Removal of color from dye wastewater is of primary importance because they are highly toxic and carcinogenic to many life forms. To protect the environment, studies need to be conducted to make the use of inexpensive adsorbent for the removal of color from dye wastewater. To the best of our knowledge, there has practically been no work reported for describing the potential of using neem leaf fine powder (NLP) as adsorbent for the decolorization of Coomassie violet (CV) from wastewater either in batch or continuous mode. The present batch study is concerned with the removal of CV dye from synthetic aqueous solutions using NLP as an adsorbent. Decolorization experiments were conducted by varying experimental factors such as initial pH, initial dye concentration, adsorbent dosage, particle size, and agitation speed. The process parameters were optimized using response surface methodology to attain the maximum % decolorization. Further, the batch experiments were conducted to study the effect of a mixture of dyes, and temperature on dye decolorization. The adsorbent was characterized by Brunauer–Emmett–Teller surface area, pore-volume, particle size, attenuated transmission reflector, field emission scanning electron microscopy/energy-dispersive X-ray spectroscopy, X-ray diffraction, and thermogravimetric analysis. The experimental equilibrium data were analyzed with various isotherm models. The results showed that the best fit was achieved with the Langmuir isotherm model with the maximum monolayer adsorption capacity (q_{max}) was 39.64 mg g⁻¹ at 303 K. Thermodynamic studies were performed to determine the change in Gibbs free energy (ΔG), change in enthalpy (ΔH), and change in entropy (ΔS) of the adsorption process. Thermodynamic parameters were evaluated using q_{max} at different temperatures. From the results, the adsorption was found to be spontaneous, endothermic in nature and favored at high temperatures. The value of ΔH and activation energy confirmed that the studied adsorption process was chemisorption. Kinetic rate constants were found using different kinetic models. The adsorption kinetics for CV dye removal by NLP adsorbent follows a pseudo-second-order kinetic model. The adsorption mechanisms were described by pore diffusion, Bangham and Boyd plots. The overall rate of adsorption was controlled by both film diffusion and pore diffusion of dye molecules. It was found that external film diffusion controlled the dye uptake in the earlier stages, followed by pore diffusion, which controlled the rate at later stages. A number of various desorbing reagents were tested to explore the possibility of regenerating the NLP adsorbent and ethanol had the maximum desorption efficiency. The reusability studies of NLP adsorbent for the adsorption of CV was carried out in three runs. The adsorption of solute from textile industrial Congo red dye effluent was carried out in batch studies using NLP adsorbent. The chemical oxygen demand removal efficiency of industrial dye effluent was 69.18%.

Keywords: Coomassie violet dye; *Azadirachta indica* (neem) leaf powder; Equilibrium; Kinetics; Isotherms; Desorption

* Corresponding author.

1. Introduction

Water is vital for life, water scarcity is becoming a global concern and its quality is closely related to human health. Nowadays, one of the key environmental problems being faced by humans is the increasing worldwide contamination of freshwater systems with thousands of industrial chemical compounds [1]. The intensive development of the industry is accompanied by a decrease in environmental quality. Although industrial development involves the implementation of environmentally accepted dyeing processes, it creates a large quantity of effluents that are discharged into the groundwater and pollute the environment [2]. Worldwide, the overall dye utilization of the textile industry is in excess of 10^7 kg/y and approximately 1 million kg of textile dyes are released as industrial wastewater per year [3]. On the other hand, about 10%–15% of textile dyes are lost in the dyeing process and 2%–20% are directly discharged as aqueous effluent in various ecological segments [4]. Currently more than 1×10^5 dyes are commercially available having various applications with global annual production in excess of 7×10^5 million tons [5]. A literature survey indicates that on an average 150–200 L of water is consumed and about 125 L of effluent is generated per kg of finished textile produced in India. It is about 1×10^6 L of effluent is discharged per day by an average-sized textile mill having a daily production of 8,000 kg of finished products [6]. Color is the first contaminant to be recognized since it is visible to the human eye. The color in the dye concentration is greater than 1 mg L^{-1} and at an average concentration of 300 mg L^{-1} [7].

The synthetic dye Coomassie violet (CV) (Acid violet) is a water-soluble anionic dye. Acid dyes are used in several industries, such as textiles, paper, printing and plastics to color their products [8]. The continuous discharge of dye effluents from these industries into the receiving water bodies creates severe environmental problems as synthetic dyes are toxic, harmful to flora and fauna in water and human beings [9]. The dyes also create significant aesthetic problems as they give obnoxious color to the water. Dyes may have carcinogenic and mutagenic effects on aquatic life [10]. The presence of dyes in water bodies would be cause to increase the value of chemical oxygen demand (COD) yields difficult for the penetration of sunlight in water bodies which in turn affects the dissolved oxygen concentration, and photosynthetic activity of aquatic plants [11]. Most of the acidic anionic dyes were reported to be the main cause for bladder cancer in humans, splenic sarcomas, hepatocarcinomas and chromosomal aberration in mammalian cells [12]. Even a low concentration of CV dye causes toxic effects and is extremely difficult to remove due to their complex structure [13]. Therefore, the removal of CV from effluents is of utmost importance to protect the environment and the aquatic life, before the discharge of the wastewater into the environment. The concentration of dye in effluent must be reduced to acceptable levels [8].

There are several treatment technologies like adsorption, chemical precipitation, ion exchange, membrane filtration, electrochemical oxidation, photo-catalytic degradation, ozonation Fenton process, sonication, biodegradation and biosorption available for the treatment of dyes bearing wastewater [9]. Many of these methods, excluding

adsorption, suffer from various drawbacks such as high capital and operating cost, complexity of the treatment processes, and the need to dispose sludge formed in the process [14]. Among the numerous treatments of color removal, adsorption is considered to be widely used technique as it provides higher efficiency especially if the adsorbent is inexpensive and readily available. This process is becoming a superior and promising technology because of its simplicity, ease of operation and handling, sludge free operation, environmentally friendly application and regeneration capacity [15]. Adsorption can indicate the electrostatic interaction between adsorbate (dye) molecules and active sites of the adsorbent. Optimized adsorption process have higher efficiency and adsorption capacity resulting in a high quality treated effluent. Most of the commercial industries use activated carbon as adsorbent to remove color from effluents [16]. However, activated carbon usage is limited due to high cost and its regeneration and reuse make it more costly [17]. However, in view of the high cost and associated problems of regeneration, there is a need for alternate low-cost, easily available and more effective adsorbents [14]. Various low-cost adsorbents from agricultural and plant waste materials have been used to remove color from aqueous solution. These adsorbents include wheat bran [18], papaya seeds [19], sugar cane bagasse [20], wheat straw [21], lotus leaf [22], and neem leaf [23]. However, studies on the removal of CV dye from wastewater using neem leaf fine powder (NLP) adsorbent is an area that has not been explored much. To the best of our knowledge, there has practically been no work reported for describing the potential of using neem leaf powder as adsorbent either in batch or continuous mode for the removal CV dye from aqueous solutions. Studies need to be conducted to make the use of inexpensive adsorbent for the removal of color from wastewater. Therefore, an effort has been made to remove CV dye from wastewater using agricultural biomass. Response surface methodology (RSM) studies were not performed earlier for optimization of experimental parameters for the removal of CV dye using NLP adsorbent. A mathematical model (kinetics and isotherm model) has to be developed in batch studies that suits the decolorization of CV from synthetic dye wastewater using NLP adsorbent. The selection of neem leaves material is based on adsorption capacity, cost and availability, etc. The neem leaves are economically viable and a most readily available natural material in India. The low cost adsorbent (agricultural by-product) have given satisfactory performance at laboratory scale for treatment of coloured effluents [24]. The neem tree (*Azadirachta indica*) of the family *meliaceae* is native to the Indian subcontinent, and its seeds and leaves were used to treat a number of human diseases and also as a household pesticide. A number of medicinal and germicidal properties of the leaves, bark, seeds and other parts are being used to treat various diseases. The neem tree serves as a natural air purifier and helps growth of other trees in barren land by improving soil fertility and preventing the loss of valuable topsoil by wind-erosion, especially during the winter [25]. The principal constituents of neem leaves include cellulose (20.64%), hemicellulose (50.84%), lignin (18.52%), lipids, protein, minerals, calcium, phosphorus, carotene, etc. [26]. Agricultural materials particularly those containing

cellulose show potential adsorption capacity for various pollutants [24]. The present study focused on an economical treatment process to remove the CV color from synthetic dye wastewater using NLP adsorbent. The effect of various factors such as initial pH, initial dye concentration, adsorbent dosage, adsorbent particle size, and agitation speed on CV color removal process were studied and the process parameters were optimized using central composite response surface design. Isotherm, thermodynamic, kinetic and desorption studies were performed using optimized value of various process parameters.

2. Materials and methods

2.1. Preparation of the NLP adsorbent

Mature neem leaves were collected from a number of tall neem trees in Karkala, Karnataka State, India. The leaves were dried under sunlight to remove the moisture and ground to NLP using pulverizer. The powdered materials were washed with distilled water to remove all the dirt particles and till the wash water was free of colour and turbidity. Then, the materials were dried in a hot-air oven at the temperature of 333 K for 24 h, ground, and screened to obtain particles <150 µm in size [25]. The materials were then stored in airtight plastic bottles for further use. No other physical or chemical treatment was used prior to the adsorption experiments.

2.2. Chemicals required

An anionic dye Coomassie violet (Dye content = 50%, Molecular formula = $C_{41}H_{44}N_3NaO_6S_2$, Molecular weight = 761.92, λ_{max} = 545 nm) supplied by Sigma Aldrich (India) was used in the study. The dye was of analytical reagent grade, and of 99.8% purity. The other anionic dyes like Congo red, Remazol brilliant blue-R, and Acid green 25 were also obtained from Sigma Aldrich (India). All other chemicals such as hydrochloric acid, sodium hydroxide, methanol, ethanol, isopropanol, and sodium chloride used were of analytical grade (Merck, India).

2.3. Preparation of CV dye stock solution

A stock solution of 1,000 mg L⁻¹ was prepared by dissolving required amount of CV dye powder in distilled water. This stock solution was further diluted with pH adjusted distilled water by adding 0.1 N HCl or 0.1 N NaOH to obtain the required concentration range. After dilution (adjusting the pH), the final pH of the dye solution was measured as required range. The structure of the CV dye is shown in Fig. S1.

2.4. Analytical measurements

The pH of the dye solution was observed by a digital pH-meter (Systronics 335, India), and the average particle size of the adsorbent was evaluated by a particle size analyzer (Cilas 1064, France). The surface area of the adsorbent was evaluated using a Brunauer–Emmett–Teller (BET) surface analyzer (Smart Instruments, India). A double-beam

UV/visible spectrophotometer (Shimadzu, Japan UV-1800) was used to determine the unknown residual concentration of CV dye solution. Attenuated transmission reflector (ATR) spectra in the transmission range of 400–4,000 cm⁻¹ was used to determine the functional groups in the NLP adsorbent and CV dye loaded with adsorbent using ATR spectroscopy (IR Prestige-21, Shimadzu, Japan). The surface morphology of adsorbent before and after adsorption was analyzed by field emission scanning electron microscopy/energy dispersive X-ray spectroscopy (FESEM/EDAX) (CARL ZEISS–FESEM attached with Oxford instruments EDAX, Germany). X-ray diffraction (XRD) (Rigaku ultima IV, Japan) analysis was used to investigate the crystalline materials. The well-defined peak shows the crystalline nature and the hallow peaks show the non-crystalline amorphous nature of the adsorbent [27]. The thermal stability of the dried NLP adsorbent and the presence of guests, thermogravimetric analysis, TGA-55, (TA instruments, England) was conducted under the following operational conditions: heating rate 283 K/min, dynamic atmosphere of argon (30 mL min⁻¹) in the temperature ranges between 323 and 973 K.

2.5. Adsorption experiments

The adsorption experiments were conducted at 303 K to study the effect of initial pH, initial dye concentration, adsorbent dosage, adsorbent particle size, agitation speed, and temperature on the adsorptive removal of CV color from aqueous solution using NLP adsorbent. Batch experiments were performed by varying the level of one factor and keeping the level of other factors constant on the other hand. Adsorption equilibrium experiments were conducted by stirring CV dye aqueous solutions at 180 rpm for 24 h at 303 K with initial dye concentration of 50–300 mg L⁻¹ in each flask containing fixed quantity of adsorbent dosage. The adsorption kinetics experiments were carried out at various adsorbate concentrations from 50 to 300 mg L⁻¹ with a fixed adsorbent dosage and at constant temperature. A known amount of solution was withdrawn at regular time intervals. Then, the samples were centrifuged (Remi CPR-24 Plus, India) at 12,000 rpm for 10 min to settle down the suspended particles [28]. After centrifugation, the clear supernatant liquid was obtained and analyzed for the residual dye concentration. The equilibrium adsorption capacity (q_e), adsorption capacity at any time t (q_t) and the % decolorization were determined using Eqs. (1)–(3), respectively [28,29]:

$$q_e = \frac{(C_0 - C_e)V}{W} \quad (1)$$

$$q_t = \frac{(C_0 - C_t)V}{W} \quad (2)$$

$$\% \text{ removal} = \frac{(C_0 - C_e) \times 100}{C_0} \quad (3)$$

where C_0 and C_e are the initial and equilibrium adsorbate concentration in the solution (mg L⁻¹), C_t is the

adsorbate concentration in the solution at time t (mg L^{-1}), V is the volume of dye solution (L), and W is the mass of dry adsorbent (g).

2.6. Experimental design and optimization of process parameters

Factorial experimental design was used to obtain the overall best optimization and to minimize the number of experimental trials. It was used to investigate the relationship between % adsorption and operating variables. The experimental design was constructed through Minitab 16 statistical software and central composite design (CCD) was applied to conduct adsorption experiments. The CCD utilizes multi-level factorial design with centre points, augmented with a group of axial (or star) points that allow the estimation of curvature to fit the quadratic model [30]. The influencing factors, such as initial pH (X_1), initial adsorbate concentration (X_2), adsorbent dosage (X_3), and agitation speed (X_4) were chosen as the independent variables while the % color removal was set as the response (dependent) variable. The numbers of experimental runs are calculated by the following Eq. (4) [31]:

$$N = 2^f + 2f + N_0 \quad (4)$$

where, f represents the number of variables, 2^f represent the number of factorial points, $2f$ represents the axial points and the center points are represented by N_0 . A total of 31 experiments were conducted including 16 factorial points, 8 axial points, and 7 center points using 2^4 full factorial design. The levels of independent variables were coded as -2 (very low), -1 (low), 0 (central point), $+1$ (high), and $+2$ (very high). The coded values of process variables were obtained from Eq. (5) [28]:

$$x_i = \frac{(X_i - X_0)}{\delta X} \quad (5)$$

where x_i is the dimensionless value of a process variable; X_i is the real value of an independent variable; X_0 is the value of X_i at the center point and δX denotes the step change. The polynomial expression for the relation between the independent and response variables is given as [32]:

$$Y = \beta_0 + \sum \beta_i x_i + \sum \beta_{ii} x_i^2 + \sum \sum \beta_{ij} x_i x_j \quad (6)$$

where Y is the predicted response variable of % decolorization; β_0 is the offset term (intercept value); and β_i , β_{ii} , and β_{ij} are the regression coefficients for linear, quadratic, and interaction effects, respectively. The sign of each coefficient indicates the direction of the relationship with response variable. Each coefficient estimates the change in the mean response per unit change in X when all other predictors are held constant. Analysis of variance (ANOVA) is a statistical technique that is widely employed to assess the significance of various variables in the decolorization process. These analysis were done by means of main effects, interaction effects, coefficients of the model, standard deviation of each coefficient, probability level, Fisher's ' F '-test, and Student ' T '-test. The probability level, P , was used to verify

the significance of each of the interactions among the factors and T -tests were applied to evaluate the significance of the regression coefficients of the parameters. Larger magnitude of $T_{\text{statistics}}$ and lower values of P ($P < 0.05$) indicates that the linear, quadratic, and interaction effects are more significant in the chosen model at the corresponding coefficient terms. The suitability of the response surface model was assessed by the values of regression coefficient (R^2), coefficient of variation, adequate precision and by the analysis of lack of fit. The value of R^2 between zero and one ($0 < R^2 < 1$) and the larger value was better. The repetition of central point were used to obtain the standard error of the coefficients [19]. The significant factors are arranged in ascending order with respect to their significance and hence the most significant factor is determined easily.

2.6.1. Residual analysis

The predicted responses obtained from RSM were compared to the actual responses, for verification of the predicted data. The root mean squares error (RMSE) and the absolute average deviation (AAD) are used to predict the adequate precision of the model equation. The lower value of RMSE and AAD yield best fit model equation. The RMSE and AAD were determined using the following Eqs. (7) and (8) [28,32]:

$$\text{RMSE} = \sqrt{\left(\frac{1}{N} \sum (Y_a - Y_p)^2 \right)} \quad (7)$$

$$\text{AAD} = \frac{1}{N} \sum \left(\frac{Y_p - Y_a}{Y_a} \right) \times 100 \quad (8)$$

where Y_a is the actual response value, Y_p is the predicted response value obtained from the RSM, and N is the number of experiments.

2.7. Adsorption isotherms

Adsorption isotherm will describe the equilibrium distribution of adsorbate molecules between the solid and liquid phases. It explains the equilibrium relationship between the amount of solute adsorbed (mg g^{-1}) and its concentration remaining in the solution (mg L^{-1}) at a constant temperature. The equilibrium data commonly known as adsorption isotherms are basic requirements for designing the adsorption systems. These data provide information on the capacity of the adsorbent or the amount required to remove the mass of solute from aqueous solution under the system conditions (to evaluate the efficacy of the prepared adsorbent). It is required to analyze the adsorbate-adsorbent interactions. It is characterized by certain constant values which express the surface properties and affinity of the adsorbent and can also be used to compare the adsorptive capacities of the adsorbent for different pollutants [33]. Various isotherm models are available from the literature to analyze the experimental adsorption data. The models are generally analyzed from the plot of q_e vs. C_e . Linear regression is commonly used to determine best fit isotherm model, and the method of least

squares has been widely used for obtaining the isotherm constants.

2.7.1. Freundlich adsorption isotherm model

The Freundlich model is based on the assumption that adsorption occurs on a heterogeneous solid surface having unequally available sites with different energies of adsorption over the surface and the possibility of multilayer adsorption. It also proposes reversible adsorption and possibility of adsorption on multilayer. It is assumed that the adsorbent-adsorbate interaction decreases leads to decrease in the binding energy with the saturation of available binding sites [3]. The linear expression of this model equation (Eq. (9)) is given by [34]:

$$\log q_e = \log K_F + \frac{1}{n} \log C_e \quad (9)$$

where K_F and $1/n$ are the Freundlich isotherm constant ($L g^{-1}$) and heterogeneity factor, respectively, which indicate the capacity and intensity of adsorption. The value of n is an indication of the favourability of adsorption. When $0 < 1/n < 1$, the adsorption is favourable; $1/n = 1$, there is no interaction among the adsorbed species; $1/n > 1$, the adsorption is unfavourable [29]. The linear plot of $\log q_e$ vs. $\log C_e$ permits the evaluation of model constants, K_F and $1/n$ from the intercept and slope of the plot.

2.7.2. Langmuir isotherm model

The Langmuir model is derived based on the following assumptions: (a) surface of the adsorbent contains a fixed number of active sites and all the adsorption active sites are equivalent. These active sites stops the adsorption of the adsorbate, (b) adsorption occurs at specific homogeneous binding sites and monolayer of adsorption is formed, (c) after completion of adsorption, no more interaction between the adsorbent and adsorbate molecules (active site become inactive once the adsorbate molecule is loaded onto adsorbent surface), (d) no interaction between adjacent solute molecules on the adsorbent surface, (e) energy of adsorption is same all over the entire surface of the adsorbent and (f) molecules adsorb at fixed binding sites and do not migrate over the surface. The linear form of Langmuir isotherm model is expressed as [35]:

$$\frac{1}{q_e} = \frac{1}{q_{\max}} + \frac{1}{q_{\max} K_L C_e} \quad (10)$$

where K_L is the Langmuir isotherm constant ($L mg^{-1}$) and q_{\max} is the saturated monolayer adsorption capacity at maximum ($mg g^{-1}$). The linear plot of $1/q_e$ vs. $1/C_e$ permits the determination of q_{\max} and K_L from the intercept and slope of the plot. The essential characteristics of the Langmuir isotherm can be expressed in terms of a dimensionless separation factor, R_L which is defined by the following Eq. (11) [36]:

$$R_L = \frac{1}{1 + K_L C_0} \quad (11)$$

The value of R_L indicates the shape of the isotherms (nature of adsorption) to be either unfavourable ($R_L > 1$), linear ($R_L = 1$), favorable ($0 < R_L < 1$) or irreversible ($R_L = 0$) [37].

2.7.3. Temkin isotherm model

The Temkin isotherm model was developed by considering the adsorbing species-adsorbate molecular interactions. This model assumes that (i) the heat of adsorption associated with the molecules on the adsorbent decreases linearly with the coverage and (ii) adsorption is by an equal distribution of maximum binding energy. A linear form of the Temkin isotherm model is represented by the by the following linear Eq. (12) [38]:

$$q_e = \frac{RT}{b_T} \ln K_T + \frac{RT}{b_T} \ln C_e \quad (12)$$

where K_T is the Temkin isotherm constant ($L g^{-1}$), RT/b_T indicates the heat of adsorption, b_T is the adsorption energy ($kJ mole^{-1}$), T is the absolute temperature (K), and R is the universal gas constant ($J mole^{-1} K^{-1}$). The plot of q_e vs. $\ln C_e$ is used to determine the isotherm constants b_T and K_T from the slope and intercept.

2.7.4. Error analysis

The chi-square (χ^2) error analysis was carried out using the experimental data for the adsorption of CV onto NLP adsorbent. It is useful to evaluate the best fit isotherm model. If the data from the isotherm model (predicted value) are similar to the experimental data, χ^2 will be a small number; if they are different, χ^2 will be a large number. The chi-square (χ^2) value was calculated using the following Eq. (13) [39]:

$$\chi^2 = \sum \left[\frac{(q_{e,\text{expt}} - q_{e,\text{calc}})^2}{q_{e,\text{calc}}} \right] \quad (13)$$

where $q_{e,\text{expt}}$ and $q_{e,\text{calc}}$ are the experimental adsorption capacities of CV ($mg g^{-1}$) at equilibrium and the corresponding values that are obtained from the isotherm models.

2.8. Effect of temperature and thermodynamic parameters

Various textile dye effluents are discharged at relatively high temperature (323–333 K); hence temperature can be an important parameter in the adsorption process for the real application of NLP adsorbent. The effect of temperature on equilibrium dye uptake (q_e) of adsorbent was studied by varying the temperature from 303 to 323 K with various concentration of dye solutions (50–300 $mg L^{-1}$). The adsorption thermodynamics is essential to investigate whether the process is spontaneous or not and also to determine nature of the adsorption process. The thermodynamic parameters such as Gibbs free energy change (ΔG), enthalpy change (ΔH), and entropy change (ΔS) of the process for the adsorption of CV dye were determined using the following Eqs. (14) and (16) [1,29]:

$$\Delta G = -RT \ln(K_a) \quad (14)$$

$$\ln K_a = \frac{\Delta S_{\text{ads}}}{R} - \frac{\Delta H_{\text{ads}}}{RT} \quad (15)$$

$$K_a = q_{\text{max}} K_L \quad (16)$$

It shows that the free energy of adsorption (ΔG) can be related with the adsorption equilibrium constant K_a (L g^{-1}) corresponding to the reciprocal of the slope ($1/(q_{\text{max}} K_L)$) of Langmuir plot (K_a is the product of maximum adsorption capacity (q_{max}) and Langmuir constant (K_L)). The values of ΔH and ΔS can be determined from the slope and intercept of the linear plot of $\ln K_a$ vs. reciprocal of temperature. The activation energy (E_a) for the adsorption of CV onto adsorbent was determined by Arrhenius relationship. The linear form of the Arrhenius equation (Eq. (17)) can be expressed as [15,40]

$$\ln K_2 = \ln A - \left(\frac{E_a}{RT} \right) \quad (17)$$

where A is the Arrhenius frequency factor. The value of K_2 was obtained by each reaction performed at various temperature with different concentration of dye solutions and the value of E_a can be determined from the slope ($-E_a/R$) of the linear plot of $\ln K_2$ vs. $1/T$. The type of adsorption phenomena is generally classified either physical or chemical based on the values of activation energy and enthalpy change. Low activation energies ($5\text{--}40 \text{ kJ mole}^{-1}$) are characteristics of physical adsorption, while higher activation energies ($40\text{--}800 \text{ kJ mole}^{-1}$) suggest chemical adsorption [41]. Similarly, if the value of $\Delta H < 25 \text{ kJ mole}^{-1}$ represent that the process may be considered as physisorption, whereas $\Delta H > 40 \text{ kJ mole}^{-1}$ suggest that the process may be occurred as chemisorption [29,42].

2.9. Kinetic studies of adsorption

A study of kinetics of adsorption is desirable as it provides information about the rate limiting step and mechanism of adsorption, which is important for efficiency of the process [43]. The rate of adsorption onto an adsorbent surface depends upon a number of parameters such as structural properties of adsorbent, initial concentrations of the solute, and the interaction between the solute and binding sites of the adsorbent [44]. Adsorption kinetics is defined as the rate at which solute is removed which controls the residence time of the pollutant in the adsorbent-liquid phase interface. It monitors the experimental conditions that control the speed of a chemical reaction and the equilibrium [45]. The prediction of batch adsorption kinetics is necessary for the design of industrial adsorption columns and to develop mathematical models to describe the process.

2.9.1. Pseudo-first-order and second-order-kinetic models

To determine the rate constants of the adsorption process, the kinetics experimental data were fitted with

Lagergren pseudo-first-order and Ho's second-order kinetic models. The pseudo-first-order model assumes that the rate of change of the adsorption of solute with time may lead to changes in the uptake capacity of the adsorbent [46]. The difference between the saturation adsorption capacity and the amount of solid uptake at any time t is the driving force for adsorption, and that the overall rate of adsorption is directly proportional to either the driving force (pseudo-first-order equation) or the square of the driving force (pseudo-second-order equation) for the adsorption process [29]. The linear forms of these two models are expressed by the following Eqs. (18) and (19) [47,48]:

Lagergren pseudo-first-order kinetic model

$$\ln(q_e - q_t) = \ln q_e - K_1 t \quad (18)$$

where K_1 is the pseudo-first-order equilibrium rate constant (min^{-1}). The values of q_e and K_1 can be determined from the intercept and slope of the linear plot of $\ln(q_e - q_t)$ vs. t .

Ho's pseudo-second-order chemisorption kinetic model

$$\frac{t}{q_t} = \frac{1}{K_2 q_e^2} + \frac{t}{q_e} \quad (19)$$

where K_2 is the equilibrium rate constant of pseudo-second-order adsorption ($\text{g mg}^{-1} \text{ min}^{-1}$). The straight-line plot of t/q_t vs. t has been analyzed by linear regression to obtain the parameters of q_e and K_2 . The initial rate of adsorption h ($\text{mg g}^{-1} \text{ min}^{-1}$) is described by the Eq. (20) [49]:

$$h = K_2 q_e^2 \quad (20)$$

The linear regression correlation coefficient (R^2) calculated from these kinetic plots was used to evaluate the applicability of these models.

2.9.2. Validity of kinetic models

The adsorption kinetics of CV onto the prepared adsorbent was verified at various initial dye concentrations. The validity of the kinetic model was evaluated by the normalized standard deviation (SD, %), given by the following Eq. (21) [50]:

$$\text{Standard deviation (\%)} = \sqrt{\frac{\sum \left[\frac{(q_{e,\text{exp}} - q_{e,\text{cal}})^2}{q_{e,\text{exp}}} \right]}{N_p - 1}} \times 100 \quad (21)$$

where N_p is the number of data points. The lower value of SD indicates the better fit of the kinetic model.

2.10. Adsorption rate mechanism

While designing a solid-liquid adsorption system, the dye molecule transfer and rate of adsorption are explained by either an external boundary film, pore diffusion or both.

The prediction of rate-determining is important for the design purpose and it is essential to understand the mass transfer mechanisms. Adsorption, whether physical or chemical, involves the mass transfer of adsorbate from the bulk solution to the particle surface. When the adsorbent is porous in nature, the transport of adsorbate to adsorbent can be explained by the following steps [32]:

- Transfer of dye molecules from bulk dye solution to hydrodynamic boundary layer surrounding the adsorbent
- External film diffusion of dye molecules from the hydrodynamic layer to the outer surface of the adsorbent
- Internal diffusion, the transport of dye molecules from the particle surface into inner sites on the pores of the adsorbent
- Adsorption of dye molecules from the binding sites into the inner surface of the pores and capillary spaces of the adsorbent

The diffusion mechanism of adsorption is explained by the intra-particle diffusion (pore diffusion) model. This model is represented by the following Eq. (22) [33]:

$$q_t = K_i t^{0.5} + C \quad (22)$$

where K_i is the pore diffusion rate constant ($\text{mg g}^{-1} \text{min}^{-1/2}$) and C is the constant. The thickness of the boundary film is given by the value of C . The values of K_i and C are determined from the slope and intercept, respectively, of the linear plot of q_t vs. $t^{1/2}$. The intercept of the plot signifies the extent of the boundary layer effect. The Boyd and Bangham kinetic expressions were used to predict the slowest step, which is the rate-limiting step in the adsorption. These two kinetic expressions were described by the following equations [15,51].

Boyd kinetic expression:

$$F = 1 - \left(\frac{6}{\pi^2} \right) \exp(-B_i) \quad (23)$$

(or)

$$B_i = -0.4977 - \ln(1 - F) \quad (24)$$

$$F = \frac{q_t}{q_e} \quad (25)$$

Where F is the ratio of solute adsorbed at any time t , and B_i is a mathematical function of F .

Bangham kinetic expression:

$$\log \left(\log \left(\frac{C_0}{(C_0 - q_t m)} \right) \right) = \log \left(\frac{k_0 m}{2.303V} \right) + \alpha \log t \quad (26)$$

where m is the weight of adsorbent used per liter of solution (g L^{-1}), α is the constant and k_0 is the Banghams constant ($\text{L}^2 \text{g}^{-1}$). The overall rate of adsorption will be controlled by the slowest, rate-limiting step, which would be either film diffusion or pore diffusion. If external transport is $>$ internal

transport indicates that the adsorption rate is governed by external film diffusion, whereas, the external transport is $<$ internal transport signifies that the rate is governed by intra-particle diffusion. In case, if external transport is the same as internal transport, the transport of ions to the boundary may not be possible at a significant rate, thereby leading to the formation of a liquid film with a concentration gradient surrounding the adsorbent particles [15]. Usually, external transport is the rate-limiting step in systems, which have (a) poor mixing, (b) low concentration of adsorbate, (c) small particle size, and (d) high affinity of the adsorbate for the adsorbent. In contrast, the intra-particle diffusion limits the overall transfer for those systems that have (a) high concentration of adsorbate, (b) good mixing, (c) large particle size of adsorbent, and (d) low affinity of the adsorbate for adsorbent [52].

2.11. Desorption studies and reusability of the adsorbent

Desorption experiments were conducted using various desorbing reagents in separate batches to explore the possibility of recovery of an adsorbent. It was investigated using various desorbing reagents, such as methanol, ethanol and isopropanol [29]. In a typical desorption experiment, the above-mentioned desorbing reagents were added to the adsorbent loaded with adsorbed dye molecules and agitated for sufficient duration in separate batches. The process was continued till the dye was desorbed by the desorbing reagent, following which the centrifugation process was used to separate the regenerated adsorbent and desorbed dye molecules. In order to determine the reusability of the adsorbent, consecutive adsorption-desorption cycles were repeated three times by using the same adsorbent [53]. The desorption for the second and third runs was carried out with 100 mL of the above-mentioned variety of reagents in separate batches. The regenerated adsorbent after desorption was collected by centrifugation and was left to dry at 333 K for 24 h. The decolorization efficiency by the regenerated adsorbent was tested in the second and third run under the optimized values of the process parameters and compared with the first use. The efficiency of desorbed dye from the adsorbent was calculated by using the following Eq. (27) [39]:

$$\text{Desorption efficiency} = \frac{\text{Amount of CV dye desorbed}}{\text{Amount of CV dye adsorbed}} \times 100 \quad (27)$$

3. Results and discussions

3.1. Characterization of the adsorbent

The BET surface area of the NLP adsorbent was obtained from adsorption of nitrogen at 77 K. The bulk density of NLP was determined by the standard operating procedure [54]. The surface area of the adsorbent and bulk density was $1.86 \text{ m}^2 \text{g}^{-1}$ and 0.453 g cm^{-3} , respectively. The pore volume was found to be $1.65 \text{ mm}^3 \text{g}^{-1}$, with the average particle size of $124.92 \text{ }\mu\text{m}$. The value of bulk density indicates that the adsorbent particles are fine in nature. After adsorption,

there were no significant changes observed in the surface area and pore volume of the adsorbent. This may be due to the desorption of dye molecules from the adsorbent surface during the regeneration of the adsorbent [55]. While determining surface area, the regeneration temperature was maintained at 353 K. The physical characteristics of the adsorbent were determined, and the results are reported in Table S1. It shows that a high volatile matter containing adsorbent burns with a long flame, high smoke and has a low calorific value. Hence, the lesser the moisture content and smaller % of ash content signify the better the quality of adsorbent. [56]. ATR spectra of the adsorbent before and after CV dye adsorption are shown in Fig. 1. The assigned functional groups are as reported in Table 1. Thus, the ATR analysis demonstrated that more hydroxyl, carbonyl, and methyl groups were present on the surface of the adsorbent. These groups may act as possible binding sites for electrostatic interactions with the anionic dye molecules.

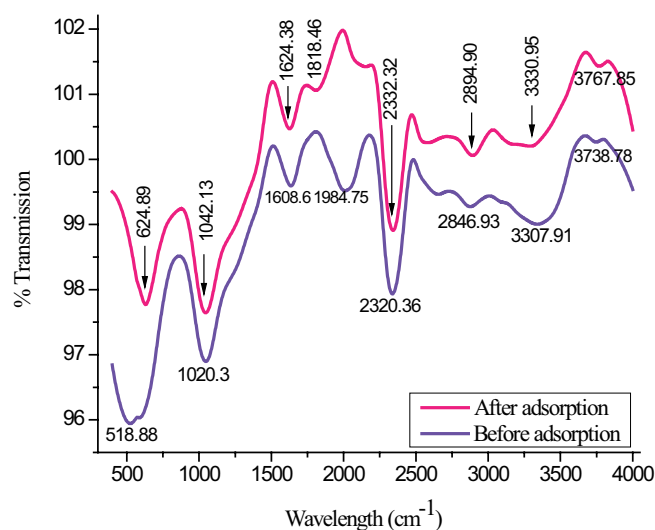


Fig. 1. ATR spectrum of NLP adsorbent before and after Coomassie violet dye adsorption.

Table 1

ATR spectral characteristics functional group assignment to observed frequencies

Sl. No.	Wavenumber of absorption		Assignment
	Before adsorption	After adsorption	
1	3,738.78	3,767.85	O–H stretching vibration in bonded hydroxyl groups (4,000–3,600 cm^{-1})
2	3,307.91	3,330.95	O–H stretching vibration in bonded carboxylic acid groups (3,400–2,500 cm^{-1})
3	2,846.93	2,894.90	C–H stretching vibration in methyl ($-\text{CH}_3$) groups (2,900–2,700 cm^{-1}) and O–H stretching vibration in bonded carboxylic acid groups (3,400–25,00 cm^{-1})
4	2,320.36	2,332.32	$\text{C}\equiv\text{N}$ stretching vibration in nitrile group (2,400–2,100 cm^{-1})
5	1,984.75	1,818.46	$\text{C}=\text{O}$ stretching vibration in anhydrides (1,900–1,800 cm^{-1})
6	1,608.60	1,624.38	$\text{C}=\text{O}$ stretching vibrations in carbonyl groups of aldehyde and ketones (1,650–1,600 cm^{-1})
7	1,020.30	1,042.13	Bending vibrations in $-\text{OH}$ group and stretching vibrations in $\text{C}-\text{O}-\text{C}$ group (1,050–1,000 cm^{-1})
8	518.88	624.89	$=\text{C}-\text{H}$ bending vibrations of alkynes (800–400 cm^{-1})

A frequency shift was observed for all band positions after CV dye adsorption [57–59]. SEM images of the adsorbent before and after adsorption of CV dye were shown in Figs. 2a and b respectively. The adsorbent had rough fibrous morphology with irregular pores which may allow for the diffusion of dye molecules through the pores of the adsorbent as seen in Fig. 2a. Rough surfaces are favorable for the adsorption of CV dye molecules onto the adsorbent [41]. The dye molecules loaded onto the adsorbent after adsorption is shown in Fig. 2b. Analytical SEM at 20 keV equipped with EDAX was used to determine the elemental composition of the adsorbent. The weight and atomic % of the elemental composition of the prepared adsorbent were reported in Table 2. EDAX analysis results revealed that the NLP adsorbent surface mainly contains the elements, carbon and oxygen (Figs. S2a and b). After adsorption the weight and atomic % of elemental carbon and oxygen increase, indicating that the surface of adsorbent is loaded with dye anions. The adsorbent was also characterized by XRD analysis using $\text{CuK}\alpha$ radiations of wavelength ($\lambda = 1.540562 \text{ \AA}$) generated at 30 KV at 30 mA. The scan measurements were performed at a 2θ range of 0° – 90° with a scan speed of $2^\circ/\text{min}^{-1}$ in step size of 0.02° [59,60]. The X-ray patterns of raw adsorbent are shown in Fig. S3. The X-ray diffraction patterns did not exhibit well-defined peaks in any region (defined peaks related to any crystalline phase), which is an indication that no discrete mineral peaks were detected in the samples. Thus, the raw NLP adsorbent had a completely amorphous structure with a noticeable hump (wide peak with low angle) in the 2θ range 20° – 30° , which signifies a high degree of disorder, typical of carbonaceous (cellulose) materials. This low angle indicated the presence of a mesoporous structure. It refers to that the particles are ordered in the preferred orientation [60]. Thermogravimetric analysis results were shown in Fig. 3. Fig. 3 shows that the weight loss consists of three distinct steps in the curves. The first stage at the low-temperature range of (323–353 K) corresponds to a rapid loss of about 5.754% of the sample weight due to non-dissociative physically absorbed water molecules as well as water held on the surface by hydrogen bonding. The weight loss at this temperature was due to

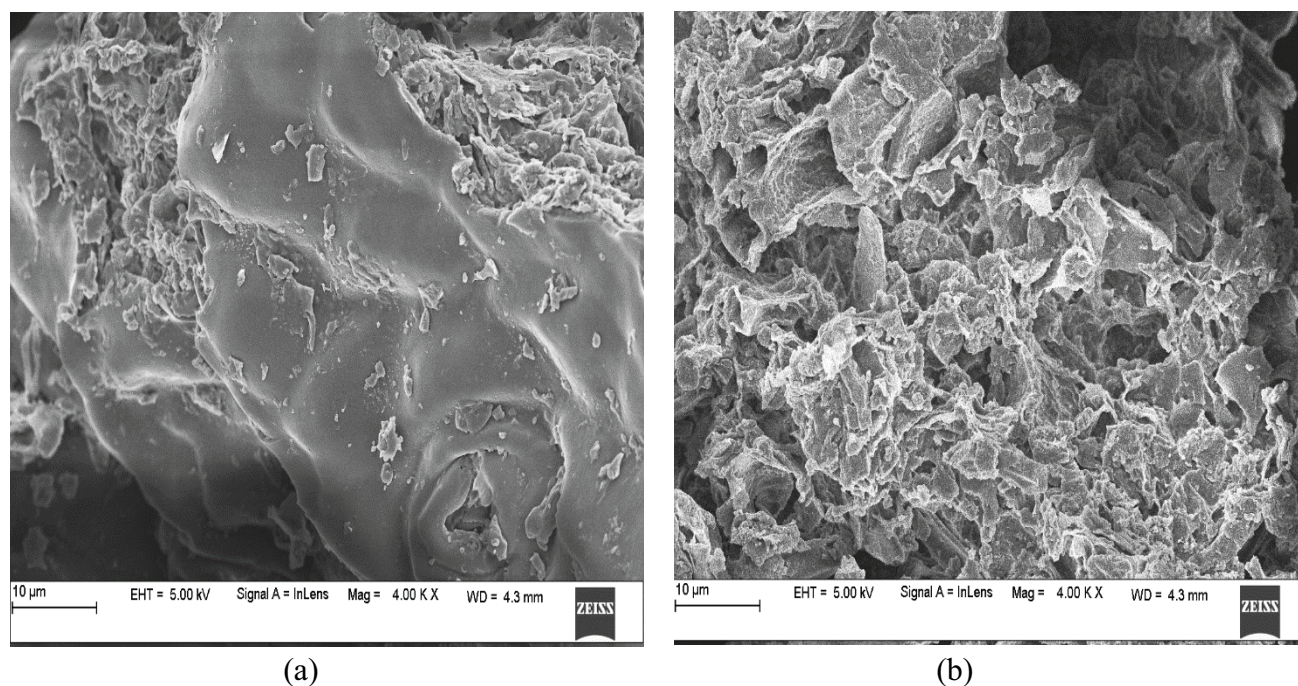


Fig. 2. SEM images of NLP adsorbent (a) before CV dye adsorption and (b) after CV dye adsorption.

Table 2
Elemental analysis of NLP adsorbent by EDAX

Process mode	Elements (weight %)			Elements (atom %)		
	Carbon	Oxygen	Calcium	Carbon	Oxygen	Calcium
Before adsorption	0.20	0.53	0.12	31.42	62.81	5.77
After adsorption	0.62	1.64	0.10	32.82	65.64	1.54

water elimination. The second weight loss is 45.479% at the temperature range of (460–633 K). This may be attributed to the degradation of cellulose/hemicellulose and lignin. In the temperature range (633–973 K) there is a third weight loss of 43.515%, which is corresponding to carbonaceous residues. A similar observation has been reported elsewhere [60].

3.2. Analysis of batch adsorption studies

3.2.1. Effect of initial pH

Adsorption of the CV dye by the NLP adsorbent is affected by the pH of the dye solution and the zero-point charge (pH_{pzc}) of the adsorbent. The pH point of zero charges of the adsorbent was determined by the powder addition method. The plot of ΔpH vs. initial pH is shown in Fig. S4. The pH_{zpc} is the initial pH when the curve crosses zero on the ΔpH scale and has been found to occur when the pH reaches 6. The presence of H^+ and OH^- ions in solution may change the potential surface charges of the adsorbent. If the pH of the solution is below the pH_{zpc} , the active sites on the surface of the adsorbent will be protonated by the presence of excess H^+ ions. If it is above its pH_{zpc} , the active sites on the surface will be deprotonated by the OH^- ions present in

the solution. At lower pH ($\text{pH} < \text{pH}_{\text{pzc}}$), the surface of the adsorbent gets positively charged. When the adsorbent is negatively charged if the pH of the solution is $> \text{pH}_{\text{zpc}}$. The effect of the initial pH on CV color removal was analyzed by varying the pH of the dye solution from 2 to 12. As shown in Fig. S5, the decolorization efficiency of CV decreased from 98.94 to 22.34% with increasing pH from 6 to 12. This phenomenon could be due to the increase in the repulsive forces between the functional groups present on the surface of the adsorbent and the CV dye molecules. As the pH of the solution increases, the active sites on the surface of the adsorbent will be deprotonated by the presence of excess OH^- ions, hence result in the number of negatively-charged sites increases (number of positively-charged sites decrease). A negatively-charged surface site on the adsorbent does not favor the adsorption of the CV dye anions due to electrostatic repulsion. Also, lower % adsorption of CV observed at basic pH may be due to competition between the excess hydroxyl ions and the negatively-charged dye ions for the adsorption active sites. The maximum decolorization of CV was found at pH 2 because of which all the experiments were carried out at this pH. At pH 2, a significant electrostatic interaction exists between the protonated adsorption sites of the adsorbent and anionic CV dye molecules.

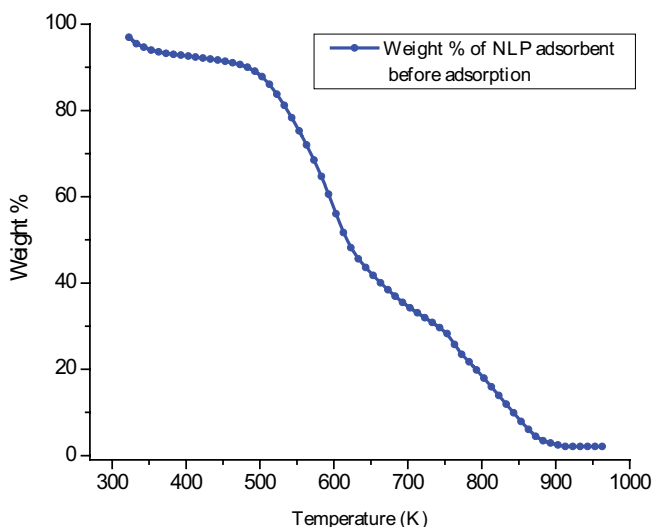


Fig. 3. TGA curve of NLP adsorbent before CV dye adsorption.

Therefore, the possible mechanisms of CV dye adsorption may be due to electrostatic interactions between protonated adsorption sites of the adsorbent and negatively charged dye anions with van der Waals forces [5,39].

3.2.2. Effect of adsorbent dosage

The effect of NLP adsorbent dosage on color removal was studied by varying the adsorbent dosage from 1–10 g L⁻¹ of dye solution with an initial dye concentration of 100 mg L⁻¹ at pH 2. From Fig. S6, it can be seen that the decolorization efficiency of CV increased from 56.72 to 99.96%, but the equilibrium dye concentration in the solution (C_e) gets decreased from 34.28 to 0.04 mg L⁻¹ with the increase in the adsorbent dosage from 1 to 10 g L⁻¹. This is because, the increase in the adsorbent dosage resulted in the increase in the availability of greater surface area and hence an increase in the number of active sites available for the adsorption of CV dye [17]. However, when the equilibrium adsorption capacity is expressed in mg dye adsorbed per gram of the adsorbent at equilibrium (q_e), the capacity decreased from 56.72 to 9.996 mg g⁻¹ with the increase in the adsorbent dosage. This is mainly due to the split in the flux or concentration gradient between the dye concentration in the solution and that at the surface of the adsorbent. Thus the competition for the availability of active sites for the adsorption of dye decreases with the increase in the adsorbent dosage (an increase of unsaturation of adsorption binding sites through the adsorption process) [15]. In other words, (i) at higher adsorbent-to-solute concentration ratios, adsorption onto the adsorbent surface is very rapid, thus producing a lower solute concentration in the solution, compared to that obtained for a lower adsorbent-to-solute concentration ratio. (ii) This may be due to, adsorbent particle interactions, such as, aggregation or overlapping of adsorption sites, resulting from high adsorbent concentration. Such aggregation would lead to a decrease in the total active surface area of the adsorbent and an increase in diffusion path length [29]. Hence, the amount of CV dye adsorbed onto a unit weight of adsorbent (q_e) gets decreased

with an increase in adsorbent dosage. Therefore, an increase in adsorbent dosage resulted in a decrease in the dye concentration in the solution.

3.2.3. Effect of adsorbent particle size

The influence of the adsorbent particle size on color removal was studied by varying the particle size from 64 to 584 μm . The results show that the decolorization efficiency of CV was dependent on the particle size. From Fig. S7, the decolorization efficiency of CV decreased gradually from 99.64% to 76.84% at 4 h with an increase in adsorbent particle size from 64 to 584 μm . The higher % adsorption with smaller particle size may be attributed to the fact that the small particles provided a larger surface area per unit mass [49]. Also, the smaller particles will have a shorter diffusion path, thus allowing the CV dye molecule to pierce deeper into the adsorbent particle rapidly, resulting in a maximum decolorization efficiency [28].

3.2.4. Effect of agitation speed

The effect of agitation speed in a batch adsorption process is important to overcome the external diffusion resistance. The influence of agitation speed on color removal was evaluated by varying the agitation speed from 0 to 225 rpm at 303 K. Fig. S8 illustrates that the color removal of CV increased from 34.26 to 99.20% with increasing agitation speed. The maximum % adsorption (99.20%) occurred at 225 rpm. Under static condition (0 rpm), the color removal efficiency was 34.26%. The increase in % decolorization may be due to enhancing in turbulence attributable to reduce the thickness of the film boundary layer (film resistance) surrounding the particles of adsorbent, thus increasing external film diffusion and uptake of CV dye molecules [29]. This phenomenon may be explained by increasing the contact surface of the adsorbent-dye solution and favoring the transfer of dye molecules to the adsorbent binding sites [28].

3.2.5. Effect of a mixture of dyes

The optimal values of various experimental factors which are obtained from CCD were used to reduce the COD of wastewater containing from a mixture of dyes such as CR, CV, Remazol brilliant blue R (RBBR), and Acid green 25 (AG 25). The effect of a mixture of dyes on COD removal was studied by contacting 100 mL mixture of above dyes of various concentrations from 50 to 300 mg L⁻¹ at room temperature (303 K). The other experimental factors were kept constant. The COD removal of a mixture of dyes decreased from 83.24% to 58.62% with an increase in the initial concentration of a mixture of dyes as shown in Fig. S9. As the initial dye concentration was increased, the available binding sites on the surface of NLP adsorbent were saturated, leading to a decrease of % COD removal. The intensity of the peaks of a mixture of dye solution was measured before and after adsorption. The intensity of peaks declined considerably after treatment using NLP adsorbent (Fig. S10). Therefore, NLP adsorbent was effectively used to decrease the pollutant level from a mixture of dyes in aqueous solution.

3.2.6. Effect of another anionic dye

The optimal values of various experimental factors which are obtained from CCD were used to remove another anionic dye, CR from aqueous solutions. The adsorption experiments were conducted using NLP adsorbent at a dye concentration of 200 mg L⁻¹ and at a temperature of 303 K. The experiment results are shown in Fig. S11. It shows that the maximum decolorization efficiency of CR was found to be 81.36% at pH 6 [15] and at 6 h. This may be due to the availability of more number of active sites on the adsorbent surface [28]. The characterization of the adsorbent suggests that the prepared material is a useful adsorbent for effective decolorization of CR from synthetic wastewater.

3.3. Analysis of factorial experimental design and optimization of process parameters

Various groups of independent variables (process parameters) were used to study the mutual effect of different variables using statistically designed experiments. The experimental ranges and levels of various independent variables in CV dye removal are given in Table 3. The comparison of predicted response values with experimental results is reported in Table 4. The results were analyzed by ANOVA and are given in Table 5. The coefficients for the linear effect of pH (X_1), initial dye concentration (X_2), and adsorbent dosage (X_3) were the first important factors ($P = 0.000$). The coefficient for the linear effect of agitation speed (X_4) did not signify the effect on color removal ($P = 0.099$). The coefficients of the quadratic effect of X_1 and X_2 were the first and second important factors ($P = 0.001$, $P = 0.002$) respectively. The coefficients of the quadratic effect of the variables X_3 and X_4 are not significant. The coefficients of the interaction effects of X_1X_2 and X_1X_3 were the first and second important factors ($P = 0.005$, 0.011). However, the coefficients of the other interactive effects (X_1X_4 , X_2X_3 , X_2X_4 , X_3X_4) among the variables did not appear to be significant. The larger value of $F_{\text{statistics}}$ indicates that most of the variation in the response can be explained by the regression model equation [28,61]. The regression model equation (Eq. (28)) for % CV dye removal is

$$\begin{aligned} \% \text{ CV removal} = & 84.34 - 4.1163 X_1 - 3.1154 X_2 + \\ & 2.9263 X_3 + 0.7188 X_4 + 1.4707 X_1^2 + 1.3895 X_2^2 - \\ & 0.1730 X_3^2 + 0.0507 X_4^2 + 1.6144 X_1 X_2 + 1.4394 X_1 X_3 - \\ & 0.1456 X_1 X_4 - 0.9781 X_2 X_3 + 0.2019 X_2 X_4 - 0.1331 X_3 X_4 \quad (28) \end{aligned}$$

The regression coefficient, R^2 quantitatively evaluates the correlation among the experimental data and the predicted

responses. The predicted values match the experimental values reasonably well with R^2 of 0.9426, which indicates that 94.26% of the variations in response could be described by this model and this also means that the model does not explain only about 5.74% of the variation. The adjusted R^2 (89.23%) is a tool to measure the excellence of fitting, but it is more appropriate for comparing models with various process parameters. It rectifies the R^2 value for the number of terms in the model and the sample size by using the degrees of freedom in its computations. Predicted R^2 (66.93%) can prevent overfitting the model and can be calculated from a predicted residual sum of squares (PRESS) statistics. A greater value of predicted R^2 indicates the models of more predictive potential. This may indicate that an overfitted model will not predict any new observations nearly as well as it fits the existing data. The term PRESS statistics is used to forecast the responses of another experiment and the lesser value of PRESS is more perfect [30,61]. The lower value of RMSE (1.444) and AAD (1.210) yield the best fit model equation. The adequacy of the model was evaluated by the residual error which is the difference between observed and the predicted response values. The variation in the response that cannot be explained by the model, and their occurrence in a normal distribution.

Fig. S12a shows that the observed standardized residuals are plotted against the expected values, given by normal distribution. The residuals in the plot follow a straight line and are normally distributed. It can be observed that the residuals from the analysis do not have any effect on the result and are the best residuals. It is a useful way to examine the hypothesis of normality of the observations. The plot of standardized residual vs. fitted values is shown in Fig. S12b. The residuals in this plot appear to be randomly scattered above and below the zero lines. The greater spread of residuals in this plot signifies the increase in the fitted values. Fig. S12c shows the histogram of the standardized residuals. A long tail in the plot indicates the skewed distribution. The one or two bars that are far from the others may be outliers. The non-uniform bars in the plot represent the more fitted values. Fig. S12d illustrates the standardized residuals in the order of the corresponding observations. It was observed that the residuals fluctuate irregularly (random pattern) around the zero lines in the order of observation, and this was used to determine the non-random error [19,32].

3.3.1. Contour and response surface plots

Response surface and contour plots were used to locate the optimum point. The contour plot indicates the mutual

Table 3
Experimental range and levels of independent variables for CV dye removal by NLP adsorbent

Independent variables	Range and level				
	-2	-1	0	1	2
Initial pH (X_1)	2	2.5	3	3.5	4
Initial dye concentration, mg L ⁻¹ (X_2)	50	100	150	200	250
Neem leaf adsorbent dosage, g L ⁻¹ (X_3)	2	4	6	8	10
Agitation speed, rpm (X_4)	140	160	180	200	220

Table 4
Four-factor full factorial CCD matrix for CV dye removal by NLP adsorbent

Run no.	X_1	X_2 (mg L ⁻¹)	X_3 (g L ⁻¹)	X_4 (rpm)	% CV color removal	
					Experiment	Predicted
1	-1	-1	-1	1	94.62	94.25
2	-1	-1	1	1	96.58	98.92
3	0	0	0	0	84.24	84.34
4	-1	1	1	1	90.22	87.91
5	0	2	0	0	80.52	83.67
6	1	-1	1	-1	90.52	89.57
7	0	0	0	0	84.36	84.34
8	-1	-1	-1	-1	93.37	92.66
9	0	0	0	-2	82.25	83.11
10	0	0	0	0	84.38	84.34
11	-1	1	-1	1	86.34	87.16
12	-2	0	0	0	99.85	98.46
13	1	1	-1	-1	79.64	77.17
14	0	0	0	0	84.28	84.34
15	-1	1	1	-1	86.39	86.04
16	-1	-1	1	-1	96.36	97.86
17	0	0	0	0	84.42	84.34
18	1	1	1	1	84.92	85.49
19	1	1	1	-1	85.48	84.21
20	0	0	0	0	84.34	84.34
21	0	0	0	2	85.06	85.98
22	1	-1	-1	-1	77.94	78.61
23	0	0	-2	0	76.24	77.80
24	1	-1	-1	1	79.41	79.62
25	0	0	0	0	84.36	84.34
26	2	0	0	0	78.82	81.99
27	0	0	2	0	89.28	89.50
28	0	-2	0	0	97.50	96.13
29	-1	1	-1	-1	84.66	84.76
30	1	-1	1	1	91.78	90.04
31	1	1	-1	1	82.12	78.98

interactions between the variables for % color removal of CV were shown in Figs. 4a–d. Fig. 4a shows that the contour plot of % color removal from the aqueous solution as a function of initial pH and dye concentration. It occurs when the dye concentration ranges between 50 and 175 mg L⁻¹, pH in the range of 2.0–3.0, and the effect is insignificant. Fig. 4b shows that the maximum predicted response occurs when the initial dye concentration ranges between 50 and 100 mg L⁻¹ and the NLP adsorbent dosage ranges from 5.5 to 10 g L⁻¹. Fig. 4c shows that the maximum predicted yield occurs when the pH ranges between 2.0 and 2.2, and the adsorbent dosage in the range of 2–10 g L⁻¹. Fig. 4d shows that the maximum predicted decolorization efficiency occurs when the agitation speed ranges between 200 and 220 rpm and the adsorbent ranges from 9.5 to 10 g L⁻¹, and the effect is not very significant. A similar observation has been reported elsewhere [28,29]. The three-dimensional response surface plot was used to understand the main and interaction effects among

the variables and to determine the optimum response level of each variable. Response surface plots are developed as a function of two factors (independent variables) while maintaining all other factors at fixed levels. The response surface curves for % color removal of CV are shown in Figs. 5a–d. Fig. 5a shows the surface plot of the response variable as a function of pH and initial dye concentration. It clearly shows that the decolorization efficiency of CV increased with the decrease in the pH and initial dye concentration. The pH in the range of 2.0–3.0 does not have a significant effect, while a dye concentration ranges between 50 and 150 mg L⁻¹ has a significant effect on the maximum decolorization of the CV using NLP adsorbent. Fig. 5b shows that with an increase in the amount of adsorbent and a decrease in pH, the % color removal improves. The response plot of pH in the range of 2.0–3.0 does not have a significant effect, while an adsorbent dosage ranges between 2 and 10 g L⁻¹ has a significant effect on the maximum adsorption of the CV dye. Fig. 5c exhibits

Table 5
ANOVA for decolorization efficiency of CV dye using NLP adsorbent from the data of CCD experiments

Term	Coefficient	SE of coefficient	$T_{\text{statistics}}$	DF	Seq SS	Adj SS	Adj MS	$F_{\text{statistics}}$	Probability
Constant	84.3400	0.7600	110.973						0.000
Regression				14	1,061.62	1,061.62	75.830	18.75	0.000
Linear				4	857.49	857.49	214.373	53.02	0.000
X_1	-4.1163	0.4104	-10.029	1	406.64	406.64	406.644	100.57	0.000
X_2 (mg L ⁻¹)	-3.1154	0.4104	-7.590	1	232.94	232.94	232.940	57.61	0.000
X_3 (g L ⁻¹)	2.9263	0.4104	7.129	1	205.51	205.51	205.511	50.83	0.000
X_4 (rpm)	0.7188	0.4104	1.751	1	12.40	12.40	12.398	3.07	0.099
Square				4	112.69	112.69	28.173	6.97	0.002
$X_1 \times X_1$	1.4707	0.3760	3.911	1	54.38	61.85	61.854	15.30	0.001
X_2 (mg L ⁻¹) \times X_2 (mg L ⁻¹)	1.3895	0.3760	3.695	1	57.32	55.21	55.208	13.65	0.002
X_3 (g L ⁻¹) \times X_3 (g L ⁻¹)	-0.1730	0.3760	-0.460	1	0.92	0.86	0.856	0.21	0.652
X_4 (rpm) \times X_4 (rpm)	0.0507	0.3760	0.135	1	0.07	0.07	0.074	0.02	0.894
Interaction				6	91.43	91.43	15.238	3.77	0.016
$X_1 \times X_2$ (mg L ⁻¹)	1.6144	0.5027	3.211	1	41.70	41.70	41.699	10.31	0.005
$X_1 \times X_3$ (g L ⁻¹)	1.4394	0.5027	2.863	1	33.15	33.15	33.149	8.20	0.011
$X_1 \times X_4$ (rpm)	-0.1456	0.5027	-0.290	1	0.34	0.34	0.339	0.08	0.776
X_2 (mg L ⁻¹) \times X_3 (g L ⁻¹)	-0.9781	0.5027	-1.946	1	15.31	15.31	15.308	3.79	0.069
X_2 (mg L ⁻¹) \times X_4 (rpm)	0.2019	0.5027	0.402	1	0.65	0.65	0.652	0.16	0.693
X_3 (g L ⁻¹) \times X_4 (rpm)	-0.1331	0.5027	-0.265	1	0.28	0.28	0.284	0.07	0.795
Residual error				16	64.69	64.69	4.043		
Lack-of-fit				10	64.67	64.67	6.467	1,732.21	0.000
Pure error				6	0.02	0.02	0.004		
Total				30	1,126.31				

Regression coefficient, $R^2 = 0.9426$, R^2 (Pred) = 0.6693, R^2 (adj) = 0.8923, $S = 2.01078$, PRESS = 372.525

Where SE, standard error of coefficient; DF, degree of freedom; Seq SS, a sequential sum of squares; Adj SS, an adjusted sum of squares; Adj MS, adjusted mean squares; PRESS, Predicted residual sum of squares; S, the value of S chart.

that the % color removal of CV increased with an increase in adsorbent dosage and a decrease in initial dye concentration. The response surface plot of adsorbent dosage ranges between 2 and 10 g L⁻¹ vs. the initial dye concentration in the range of 50–250 mg L⁻¹ shows a significant effect on color removal. Similarly, Fig. 5d shows that with an increase in the agitation speed and adsorbent dosage, the decolorization efficiency improves. The response surface plot of agitation speed in the range of 140–220 rpm vs. the adsorbent dosage in the ranges between 2 and 10 g L⁻¹ shows a significant effect on color removal of CV from aqueous solution. The optimal response values found from these plots are closely related to those values acquired from the experiment and regression model equation.

3.3.2. Process model validation

Five solutions with different values of ideal conditions have been utilized to predict the optimal conditions for CV dye removal by NLP adsorbent which is shown in Table 6. Experiments were done under fixed conditions and the results were compared to the predicted responses. The maximum decolorization efficiency (96.58%) was obtained in experiment number 3, compared to the other four experiments. The experimental value was good and compared to the predicted value of 98.64% attained using the regression

model equation. The optimal values of the process independent variables for maximal % of CV color removal are given in Table 7. The comparison between actual and predicted responses shows a good relationship between them, and it suggests that the empirical model obtained from the design could be well used for explaining the relation between various independent variables and the response in CV dye decolorization. The optimization studies clearly revealed that RSM was one of the suitable methods to optimize the best operating condition to maximize the % color removal. A similar observation has been reported elsewhere [28,31].

3.4. Inference from adsorption isotherm models

The linear form of Langmuir, Freundlich, and Temkin isotherms plots are shown in Figs. 6, S13 and S14, respectively and the results of model parameters obtained at 303 K from regressive analysis of these plots were given in Table 8. From Table 8, the higher value of the regression coefficient ($R^2 = 0.9997$) and lower value of chi-square ($\chi^2 = 0.1016$) were found in the Langmuir model, compared to the Temkin isotherm ($R^2 = 0.9856$, $\chi^2 = 3.539$) and Freundlich ($R^2 = 0.9594$, $\chi^2 = 6.144$) models. It suggests that the experimental equilibrium data for CV dye removal by NLP adsorbent was fitted very well with the Langmuir model compared to other isotherm models. According to the assumption of Langmuir

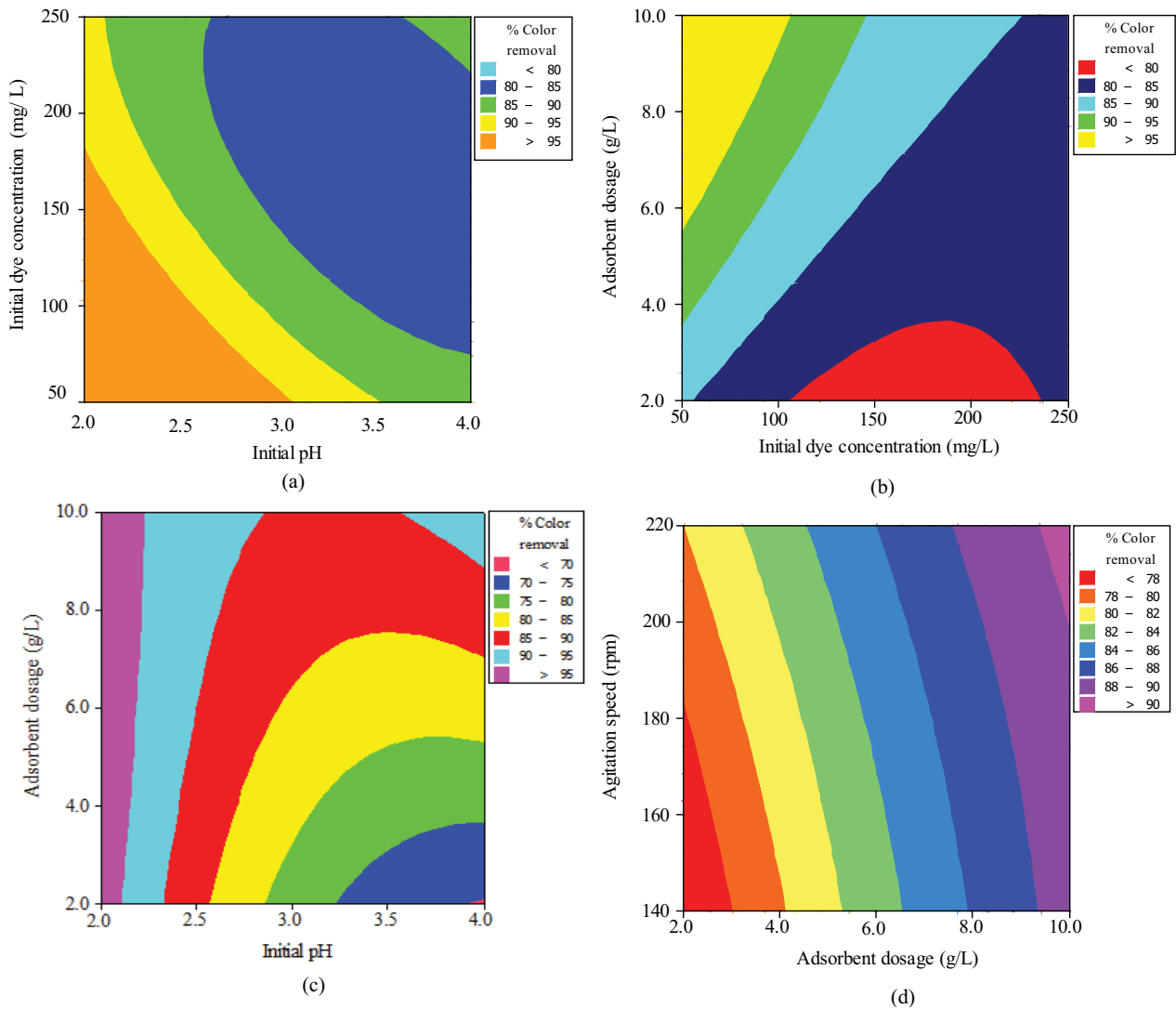


Fig. 4. Contour plots for the interactive effect of (a) initial dye concentration and pH, (b) adsorbent dosage and initial dye concentration, (c) adsorbent dosage and initial pH, and (d) agitation speed and adsorbent dosage.

isotherm, the surface of the adsorbed layer is unimolecular [29,40]. The maximum monolayer capacity of the adsorbent (q_{\max}) and Langmuir constant (K_L) at 303 K were estimated as 39.64 mg g^{-1} and 0.873 L mg^{-1} , respectively. This proves that 1 g of the prepared adsorbent could adsorb 39.64 mg of CV dye. In this case, the Freundlich model represents the poorer fit of experimental data than the other isotherm equations tested. The reason for a better agreement of data with Langmuir isotherm may be due to the homogeneous distribution of active sites on the adsorbent surface. The separation factor, R_L values obtained at various initial dye concentrations are shown in Fig. S15 of. It shows that the R_L values are in the range between 0.0038 to 0.022 indicating the adsorption is a favorable process. The values of R_L decreased from 0.022 to 0.0038 with an increase in initial dye concentration. At higher concentration, the adsorption process was found to be more favorable. The value of Freundlich constant, n (3.3045) is in-between 1 to 10 which again proved that the adsorption is favorable.

3.4.1. Comparison of adsorption capacity (q_{\max}) with other adsorbents for the removal of acid violet dye

The maximum monolayer adsorption capacities (q_{\max}) of several adsorbents for the removal of acid violet dye was reported in Table 9. It was inferred from the table that the prepared NLP adsorbent has superior adsorption capacity (39.64 mg g^{-1}) compared to other reported adsorbents. The results revealed that the NLP adsorbent as a promising adsorbent for the removal of acid violet from aqueous solutions.

3.5. Inference from the effect of temperature and thermodynamic analysis for the adsorption of CV

The effect of temperature on equilibrium dye uptake (q_e) of adsorbent was studied by varying the temperature from 303 to 333 K with various concentrations of adsorbate from 50 to 300 mg L^{-1} and the results are shown in Fig. 7. It was found that the equilibrium adsorption capacity increased

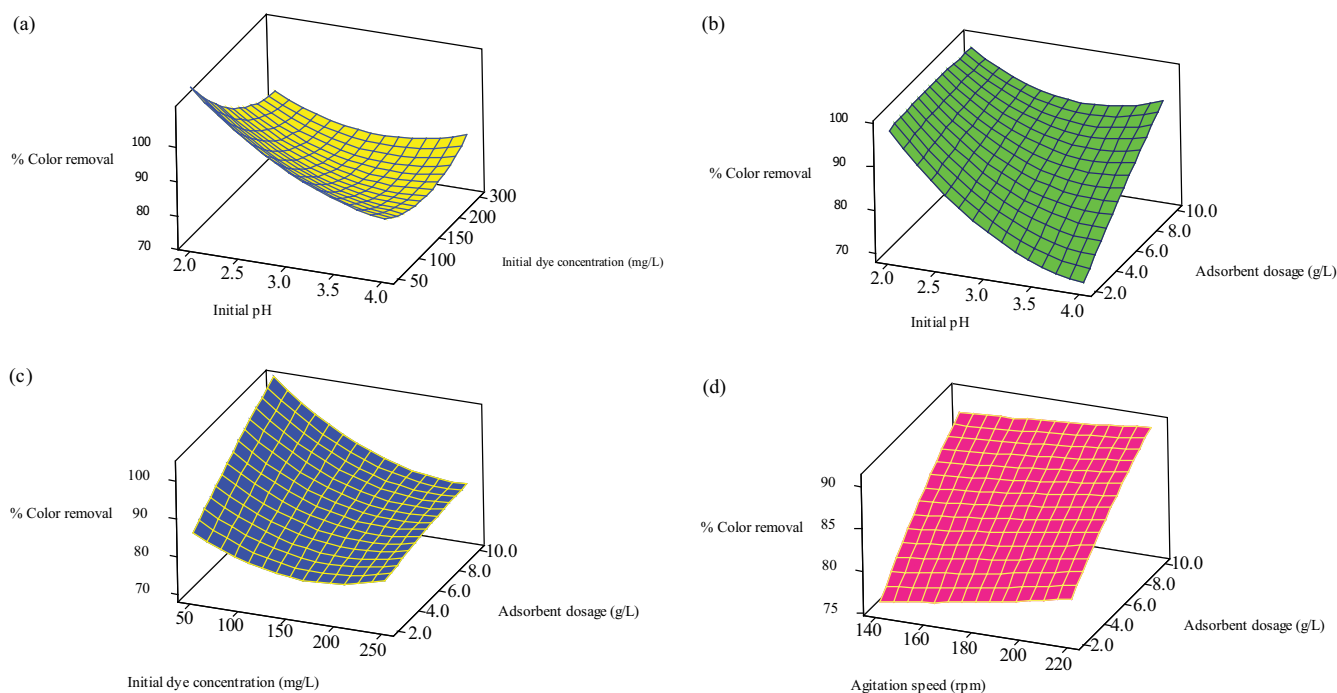


Fig. 5. Response surface plots for the interactive effect of (a) initial dye concentration and pH, (b) adsorbent dosage and initial pH, (c) adsorbent dosage and initial dye concentration, and (d) adsorbent dosage and agitation speed.

Table 6
Validation of process model

Expt.	Process parameters with operating conditions				CV color removal (%)	
	X_1	X_2 (mg L ⁻¹)	X_3 (g L ⁻¹)	X_4 (rpm)	Actual value	Predicted value
1	3.5	100	8.0	160	90.52	91.36
2	3.0	150	6.0	180	84.34	85.22
3	2.5	100	4.0	160	93.37	94.08
4	3.5	100	4.0	200	79.41	79.82
5	2.5	100	8.0	200	96.58	98.64

Table 7
Optimal values of the process independent variables for maximum % color removal of CV dye

Process parameters	Optimum value	CV color removal (%)
Initial pH (X_1)	2.0	
Initial dye concentration, mg L ⁻¹ (X_2)	150	
Neem leaf adsorbent dosage, g L ⁻¹ (X_3)	6.0	99.85
Agitation speed, rpm (X_4)	180	

from 40.234 to 49.636 mg g⁻¹ with the increase in temperature which suggests that adsorption is an endothermic process. The maximum adsorption capacity, q_{max} of adsorbent increased from 39.635 mg g⁻¹ at 303 K to 50.196 mg g⁻¹ at 333 K. This phenomenon may be due to an increase in the mobility (rate of diffusion) of CV dye molecules across the boundary layer and in the internal pores of the adsorbent particle, may be due to the decrease in the viscosity of the solution

with increasing temperature [15]. An increasing number of dye molecules may also acquire sufficient energy to undergo an interaction with active sites at the adsorbent particle surface [29]. The increase in dye uptake at higher temperatures might be due to (i) chemical interaction between dye molecules and adsorbent (ii) generation of some new adsorption binding sites in the particle surface (iii) increased rate of intra-particle diffusion of CV dye molecules into the pores of

Table 8
Adsorption isotherm model parameters for CV dye adsorption onto NL adsorbent

Isotherm	Model parameters	Values	Model equation
Freundlich	n	3.3044	$q_e = 15.0706C_e^{0.3026}$
	K_F (L g ⁻¹)	15.0706	
	R^2	0.9594	
	χ^2	6.144	
Langmuir	q_{\max} (mg g ⁻¹)	39.6353	$q_e = 34.625C_e / (1 + 0.8736C_e)$
	K_L (L mg ⁻¹)	0.8736	
	R^2	0.9997	
	χ^2	0.1016	
Temkin	K_T (L g ⁻¹)	13.2401	$q_e = 5.8854 \ln(13.24C_e)$
	b_T (kJ mole ⁻¹)	0.4280	
	R^2	0.9856	
	χ^2	3.539	

Table 9
Comparison of maximum monolayer CV dye adsorption capacity of various adsorbents determined by Langmuir adsorption isotherm model

Adsorbent	Maximum adsorption capacity q_{\max} (mg g ⁻¹)	References
Fly ash	0.45	[63]
Polyaniline-Fe ₂ O ₃ magnetic nano-composite	0.99	[64]
Red mud	1.37	[65]
Lignite coal	1.52	[63]
Kapok fruit shell carbon	1.78	[63]
Cashew nut shell carbon	1.98	[63]
<i>Penicillium</i> sp.	4.32	[66]
Polyaniline coated charcoal	4.68	[67]
Iron chromium oxide	6.49	[63]
Coir pith	8.06	[68]
Banana pith	13.10	[69]
Orange peel	19.88	[70]
Brick kiln ash	33.57	[71]
Used tea leaves charcoal	37.72	[71]
Wheat straw charcoal	37.86	[71]
Bagasse charcoal	38.32	[71]
Cement kiln ash	38.39	[71]
Neem leaf fine powder	39.64	Present work

the adsorbent. Furthermore, the increasing temperature may produce a swelling effect within the internal structure of the adsorbent enabling more dye molecules to penetrate further [28,62].

The thermodynamic parameters were calculated by plotting $\ln K_a$ vs. $1/T$ (Fig. 8), and the values are reported in Table 10. It shows that the values of ΔG decreased ($\Delta G < 0$) with the increase in temperature, suggesting that the adsorption was a spontaneous process. The values of ΔG become more negative with increasing temperature, signifies that higher temperature facilitates the adsorption of dye molecules. The positive value of ΔH ($\Delta H > 0$) again

proved that the adsorption of CV onto the adsorbent was an endothermic process. The positive value of ΔS ($\Delta S > 0$) suggests that the increased randomness of dye molecules at the particle surface than in the dye solution. The activation energy (E_a) of adsorption was determined from the Arrhenius plot (Fig. S16) and found to be 47.54 kJ mole⁻¹ with a dye concentration of 200 mg L⁻¹ (E_a values are found in the range between 45.56–47.54 kJ mole⁻¹ at various initial dye concentrations. It is given in Table S2). The value of ΔH (44.836 kJ mole⁻¹) and activation energy (46.65 kJ mole⁻¹) indicates that CV dye adsorption onto the NLP adsorbent was chemisorptive process [41,42]. It is confirming that the

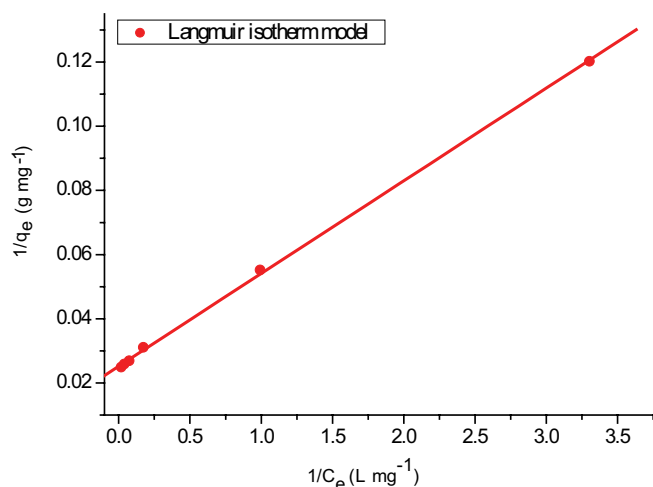


Fig. 6. Langmuir isotherm plot for adsorption of CV dye onto NLP adsorbent. (Initial pH: 2; initial dye concentration: 50–300 mg L⁻¹; adsorbent dosage: 6 g L⁻¹; adsorbent particle size: 125 μm; agitation speed: 180 rpm; temperature: 303 K; contact time: 24 h).

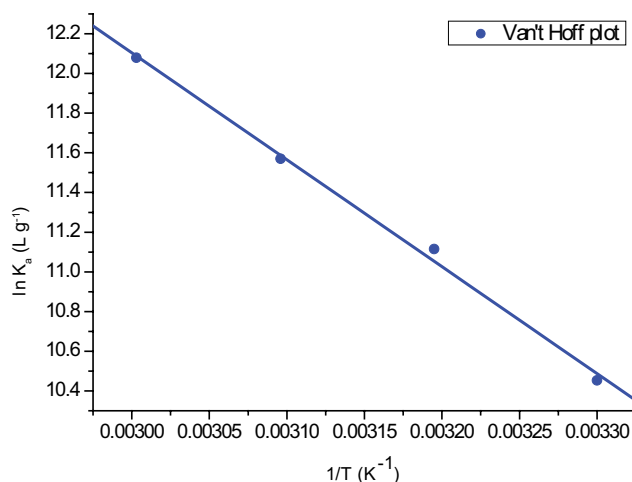


Fig. 8. Van't Hoff plot for adsorption of CV dye onto NLP adsorbent. (Initial pH: 2; initial dye concentration: 50–300 mg L⁻¹; adsorbent dosage: 6 g L⁻¹; adsorbent particle size: 125 μm; agitation speed: 180 rpm; contact time: 24 h).

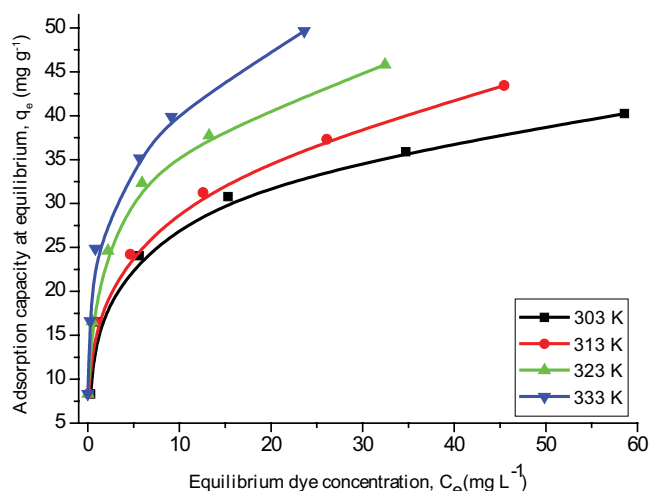


Fig. 7. Effect of temperature on adsorption of CV dye onto NLP adsorbent. (Initial pH: 2; initial dye concentration: 50–300 mg L⁻¹; adsorbent dosage: 6 g L⁻¹; adsorbent particle size: 125 μm; agitation speed: 180 rpm; contact time: 24 h).

stronger bonding forces acting between CV dye molecules and active sites on the adsorbent at higher temperatures [1,29]. CV adsorption was favored at a higher temperature, even though the process of dye uptake onto the particle surface is rapid and endothermic in nature.

3.6. Inference from adsorption kinetic models

Kinetic studies for the adsorption of CV onto the NLP adsorbent was fast in the beginning stages of the adsorption process. However, the dye removal rate later decreased gradually with time. The adsorbent surface saturated approximately 2 h for 50 mg L⁻¹, 3 h for 100 mg L⁻¹, 4 h for 150 mg L⁻¹, 5 h for 200 mg L⁻¹, 6 h for 250 mg L⁻¹ and 7 h for 300 mg L⁻¹.

Fig. S17 shows that the adsorption capacity at equilibrium (q_e) increased from 8.313 to 40.234 mg g⁻¹, but the decolorization efficiency of CV gradually reduced from 99.76% to 80.47% with the increase in dye concentration from 50 to 300 mg L⁻¹. The increase in the value of q_e is due to an increase in concentration gradient between the dye concentration in the solution and the surface of the adsorbent. This concentration gradient acts as a driving force for the transfer of dye molecules from the bulk solution to the particle surface [72]. As the initial dye concentration was increased, the vacant sites on the surface of the adsorbent were saturated (accumulation of dye molecules in the vacant sites) and the competition between more dye molecules at the fixed binding sites of the adsorbent (i.e., enhances the interaction between dye molecules and active sites on the adsorbent surface, therefore, lack of available active sites in the adsorbent surface), leading to decrease of the % decolorization [73].

The plots for pseudo-first-order and pseudo-second-order kinetic models were shown in Figs. S18 and Fig. 9, respectively and the results of the kinetic model parameters evaluated from these plots were given in Table 11. From Table 11, it was observed that the lower SD (<1.35%), higher R^2 values (closer to 1) of pseudo-second-order model and the close agreement between its predicted and experimental q_e values at various initial dye concentrations. These proved that the experimental data were well-fitted with the pseudo-second-order kinetic model for adsorption of CV onto NLP adsorbent. The value of R^2 , SD and equilibrium dye uptake shows that the pseudo-first-order model is not good in predicting the kinetics of CV adsorption. The calculated q_e of the pseudo-first-order model was much smaller than the experiment obtained q_e , which can be attributed to the existence of a boundary layer or the mass transfer resistance from outside at the beginning of adsorption [43]. Since the kinetic studies were well explained by the pseudo-second-order model, it can be assumed that the adsorption of CV dye onto adsorbent was a chemisorption process. The adsorption experiments were carried out at pH 2. The zero-point charge

Table 10
Thermodynamic parameters for the adsorption of CV dye onto NLP adsorbent

Temperature (K)	Maximum adsorption capacity q_{\max} (mg g ⁻¹)	Thermodynamic parameters		
		ΔG (kJ mole ⁻¹)	ΔH (kJ mole ⁻¹)	ΔS (kJ mole ⁻¹ K ⁻¹)
303	39.635	-26.331		
313	43.226	-28.701		
323	46.582	-31.070	44.837	0.2352
333	50.196	-33.440		

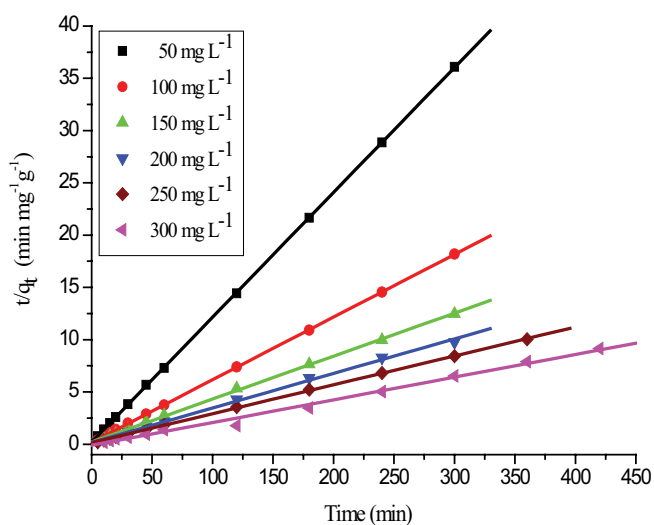


Fig. 9. Ho's pseudo-second-order kinetic plot for adsorption of CV dye onto NLP adsorbent. (Initial pH: 2; initial dye concentration: 50–300 mg L⁻¹; adsorbent dosage: 6 g L⁻¹; adsorbent particle size: 125 μ m; agitation speed: 180 rpm; temperature: 303 K; contact time: 24 h).

of the adsorbent was found to be at pH 6. Therefore, at pH 2, the surface of the adsorbent will be positively charged which facilitates the binding of negatively charged anionic dye. Hence the adsorption of CV dye onto NLP adsorbent was chemisorption involving strong valence forces through sharing or the ion exchange of electrons between the adsorbent and dye molecules as covalent forces [15,29]. Therefore, the overall rate of the dye adsorption process appears to be controlled by the chemisorption process. The chemisorption mechanism which is involved in the studied adsorption process was further confirmed by the activation energy (E_a) and change in enthalpy (ΔH) was discussed in section 3.5. The rate constant, K_2 , decreased from 0.0687 to 0.00484 g mg⁻¹ min⁻¹ as the dye concentration was increased from 50 to 300 mg L⁻¹. This is because of the decreased competition for the binding sites at lower concentrations and increased competition at the surface sites of the adsorbent at higher concentrations [44]. While the initial adsorption rate (h) of the pseudo-second-order model presented as the opposite trend. The values of h increased from 4.815 to 8.594 mg g⁻¹ min⁻¹ with an increase in initial dye concentration. This may be attributed to the increase of driving force between the liquid and solid phases with the increasing CV dye concentration. A similar observation has been reported elsewhere [15].

3.7. Possible interactions between the CV dye and the NLP adsorbent

In order to understand the adsorption process of CV dye onto the NLP adsorbent, a mechanism of adsorption is essential. In fact, the process of adsorption is controlled by various factors such as the nature of functional groups present in the adsorbent, the structural and surface properties of the adsorbent, diffusion behavior of adsorbate towards the adsorbent, and the mode of their interaction. Indeed, the adsorption of dye occurs through physisorption or chemisorption, depending on the nature of mutual interaction between adsorbent surface and adsorbate. In many cases, the accumulation of dye on agricultural biomass materials happens due to the involvement of many interactions such as Π - Π interaction, electrostatic interaction, and hydrogen bonding, which can occur during the adsorption process. CV is an anionic dye that contains a sulfonic group in its structure, which ionizes in aqueous solution, forming colored anions, together with aromatic rings. The amount of ($-\text{SO}_3^-$) anions is an important factor for adsorption of CV. The principal constituents of neem leaves include cellulose (20.64%), hemicellulose (50.84%), lignin (18.52%), lipids, protein, minerals, calcium, phosphorus, carotene, etc. Agricultural materials particularly those containing cellulose show potential adsorption capacity for various pollutants. The major mechanism of anionic dye and aromatic rings of NLP adsorbent is proposed to be chemical adsorption through the strong Π - Π stacking and anion-cation interaction. The proposed mechanism for adsorption of CV dye onto NLP adsorbent is shown in Fig. 10. The ATR analysis demonstrated that more hydroxyl, carbonyl, and methyl groups are present on the surface of the adsorbent. These groups may interact with the Π electron of the aromatic ring of the CV dye molecules. The adsorption of CV dye can take place at the functional groups or binding sites on the surface of the adsorbent in a monolayer manner. Fig. 10 shows that the hydroxyl species getting involved in the binding of dye molecules on the surface of the adsorbent. A similar type of mechanism is also reported in the literature [74]. In addition, film diffusion and pore diffusion models have been used for examining the diffusion mechanism.

3.8. Inference from adsorption rate mechanism

The intra-particle diffusion plot for the adsorption of CV onto the NLP adsorbent is shown in Fig. 11 and the model parameters were reported in Table 12. From Fig. 11, the plot of q_t vs. $t^{1/2}$ consists of two linear portions with different

Table 11
Kinetic parameters for the adsorption of CV dye onto NLP adsorbent

Initial dye concentration (mg L ⁻¹)	$q_{e,expt}$ (mg g ⁻¹)	Pseudo-first-order kinetic model				Pseudo-second-order kinetic model				
		$q_{e,calc}$ (mg g ⁻¹)	K_1 (min ⁻¹)	SD (%)	R^2	$q_{e,calc}$ (mg g ⁻¹)	h (mg g ⁻¹ min ⁻¹)	K_2 (g mg ⁻¹ min ⁻¹)	SD (%)	R^2
50	8.313	3.142	0.0607	23.517	0.9257	8.372	4.815	0.0687	0.27	0.9999
100	16.499	4.839	0.0293	24.986	0.8923	16.675	5.042	0.0182	0.38	0.9999
150	24.063	7.144	0.0144	23.437	0.8775	24.337	6.112	0.0103	0.38	0.9996
200	30.781	8.324	0.0078	23.070	0.7735	30.294	6.637	0.0072	0.50	0.9992
250	35.882	11.123	0.0062	20.805	0.9528	36.179	7.512	0.0057	0.25	0.9998
300	40.234	14.232	0.0045	18.657	0.9216	42.118	8.594	0.0048	1.35	0.9964

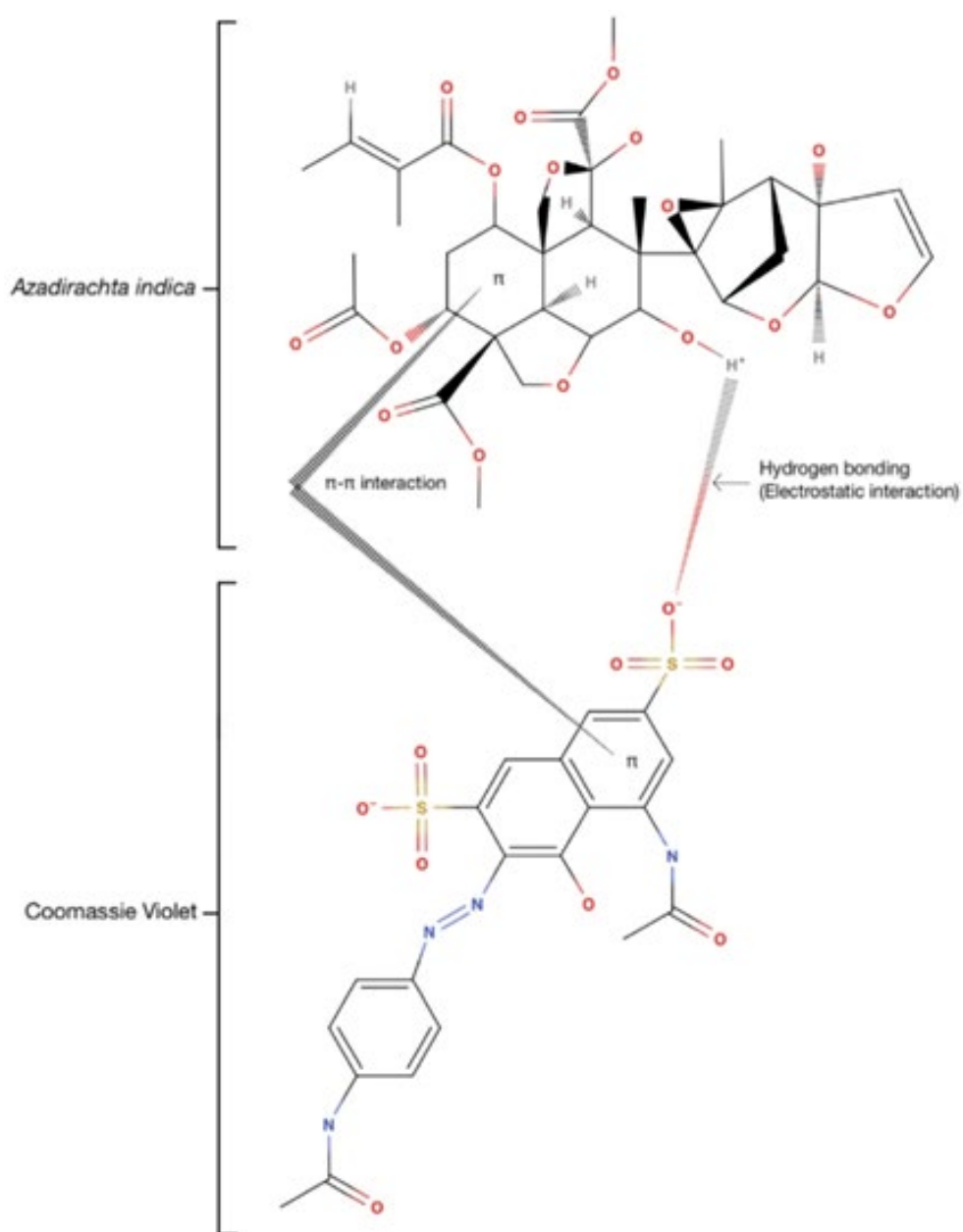


Fig. 10. Proposed mechanism for CV dye adsorption onto NLP adsorbent.

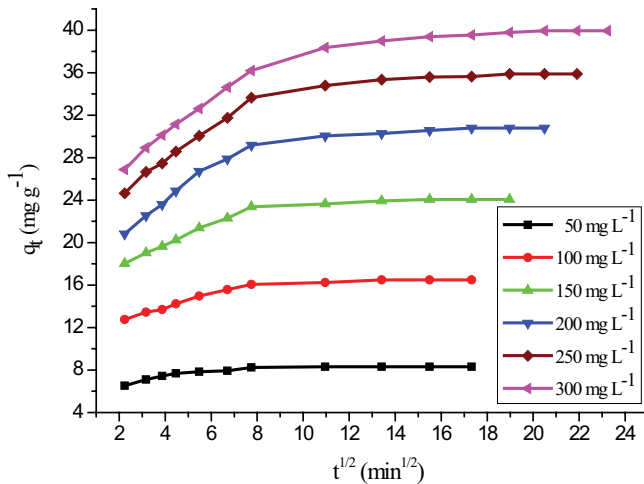


Fig. 11. Intra-particle diffusion plot for adsorption of CV dye onto NLP adsorbent. (Initial pH: 2; initial dye concentration: 50–300 mg L⁻¹; adsorbent dosage: 6 g L⁻¹; adsorbent particle size: 125 μm; agitation speed: 180 rpm; temperature: 303 K; contact time: 24 h).

slopes. The multilinearity indicates that two or more steps occur in the adsorption process. The first linear portion follows the external mass transfer diffusion (macro-pore diffusion) of the adsorbate (phase I) and the second linear portion follows intra-particle (pore) diffusion (micro-pore diffusion) effects (phase II) [15,51]. The first linear portion indicates that the diffusion rate parameters may vary with dye concentration. The second linear portion represents that, the diffusion rate parameters may not depend on the dye concentration. In phase (I), more than 67% of CV was taken up by the adsorbent within a $t^{1/2}$ value of 7.8 min. This is attributed to the instantaneous utilization of the most readily available adsorbing sites on the surface of the adsorbent. In phase (II) may be attributed to very slow diffusion of the adsorbate from the surface film into the micro-pores, which are the least accessible sites of adsorption. This also leads to a very slow rate of migration of CV from the liquid phase onto the adsorbent surface. Also, the linear plot did not pass through the origin for all the concentrations indicating that the intra-particle diffusion was not only a rate-controlling step [75]. Extrapolation of the second linear portion back to the y -axis gives the value of intercept C . The intercept of the plot reflects the boundary layer effect. A larger external

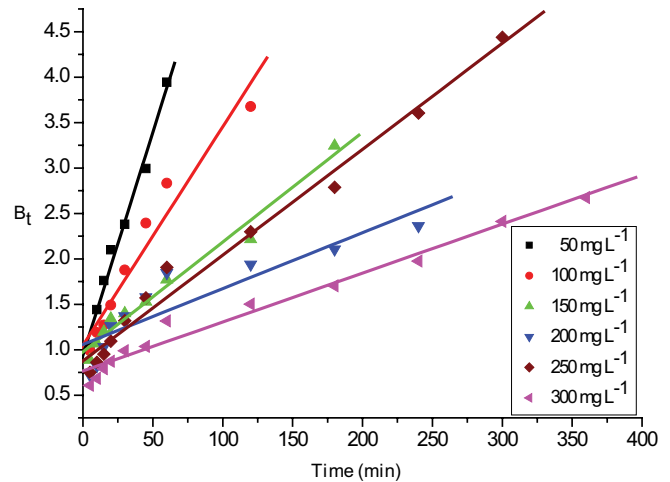


Fig. 12. Boyd plot for adsorption of CV dye onto NLP adsorbent. (Initial pH: 2; initial dye concentration: 50–300 mg L⁻¹; adsorbent dosage: 6 g L⁻¹; adsorbent particle size: 125 μm; agitation speed: 180 rpm; temperature: 303 K; contact time: 24 h).

film diffusion effect is indicated by a large intercept value. The decrease in intercept value suggests that the adsorption process is mostly governed by pore diffusion, with a slight effect of boundary layer diffusion. Therefore, the overall rate of the adsorption is mostly governed by external film diffusion, followed by a minor effect of pore diffusion of dye anions to the inner surface (both film diffusion and pore diffusion of dye molecules). It was found that the dye uptake may be controlled due to external film diffusion at earlier stages and as the adsorbent particles are loaded with dye molecules, it may be controlled due to pore diffusion at later stages. The Bangham and Boyd kinetic expressions were used to further analyze the adsorption kinetic data. The Boyd plot (Fig. 12) and Bangham plot (Fig. S19) were found to be a straight line that did not pass through the origin. This suggests that external film diffusion mainly controls the overall rate of the reaction.

3.9. Inference from desorption studies and reusability of NLP adsorbent

Desorption experiments were performed for the removal of CV from NLP adsorbent and results were shown in Fig. S20 and Table S3. It shows that the amount of CV dye

Table 12
Intra-particle diffusion constants for different initial CV dye concentrations

Initial dye concentration (mg L ⁻¹)	Intra-particle diffusion model		
	K_i (mg g ⁻¹ min ^{-1/2})	C (mg g ⁻¹)	R^2
50	0.0078	8.210	0.9058
100	0.0504	15.708	0.9316
150	0.0652	22.947	0.9439
200	0.1225	28.515	0.9396
250	0.1345	33.136	0.9478
300	0.1265	34.249	0.9534

desorbed decreased with an increasing number of runs. The % desorption in all the runs was determined to be in the order of ethanol > methanol > isopropanol with various desorbing reagents in separate batches. It was found that up to a maximum of 57.534% of the dye could be desorbed using the solvent ethanol in the third run, compared with other desorbing reagents. This may be due to the low volume of the desorbing reagent or lack of agitation speed, which may prevent further release of bound dye anions to the solvent [15,29].

The regenerated NLP adsorbent was added to the dye solution of concentration 200 mg L⁻¹. The regenerated adsorbent was tested in the second and third runs. The results obtained from reusability studies for the adsorption of CV in various runs are shown in Fig. S21 and Table S4. It shows that, in comparison to the first run, 81.864% adsorption was maintained after 24 h in the second run and 69.016% in the third run. This may be due to the incomplete desorption of the bound dye anions from the adsorbent binding sites (adsorbent active sites are almost blocked with CV dye molecules) and lack of binding sites on the adsorbent particle surface [7,29]. Therefore, the dye adsorption % gradually decreased with an increase in the number of runs.

3.10. Analysis of industrial CR dye effluent using NLP adsorbent

The real textile CR dye effluent was collected from Bright Traders, Erode District, Tamilnadu State, India. The analysis of physico-chemical parameters of real industrial CR dye effluent was given elsewhere [7]. The industrial raw effluent was centrifuged to separate the salt content, and dispersed solids, due to the high COD value of the effluent (1,824 mg L⁻¹). The pH of the raw effluent was 8.64. The optimized value of various process parameters which is obtained from CCD was used to remove COD from industrial CR dye effluents. The inlet adsorbate concentration was measured and it was found to be 200 mg L⁻¹ and the COD removal efficiency of industrial dye effluent was 69.18%. The intensity of the peaks of dye effluent was measured before and after adsorption. The intensity of peaks declined considerably after treatment using NLP adsorbent (Fig. S22). The above results showed that the NLP is a useful adsorbent for effective decolorization of CR from industrial effluents.

4. Conclusion

The present study shows that the NLP may be used as a potential adsorbent for the removal of CV dye from an aqueous solution. The prepared adsorbent was characterized by particle size, zero-point charge, surface area, functional group, surface morphology, elemental composition, amorphous nature, thermal stability, and proximate analysis using appropriate instrumental analysis. The peaks in ATR studies revealed that the surface of the adsorbent material contains abundant hydroxyl, methyl, and carbonyl groups. The decolorization efficiency of CV on NLP adsorbent was found to be strongly dependent on various experimental factors, such as initial pH, initial dye concentration, adsorbent dosage, adsorbent particle size, and agitation speed was optimized using factorial experimental design. A central composite design was used to find the optimum process

conditions to maximize color removal with a minimum number of experiments. The predicted response values fitted well with the actual values ($R^2 = 0.9426$, RMSE = 1.444, and AAD = 1.210). ANOVA confirms the accuracy of the model by using a larger value of F, lower value of P, non-significant lack of fit, and the maximum value of the regression coefficient. A removal percentage of 99.85% was attained, which was good compared to the predicted value of 98.46% using the regression model equation. This shows that the quadratic model properly explains the influence of the chosen variables on CV dye removal by the NLP adsorbent system. The % color removal of CV decreased with an increase in initial pH, initial dye solution concentration and adsorbent particle size. It increased with an increase in adsorbent dosage agitation speed and temperature. The equilibrium adsorption capacity (q_e) was found to increase with an increase in initial dye concentration and temperature but decreased with an increase in adsorbent dosage. The experimental data were analyzed using Freundlich, Langmuir, and Temkin isotherms models. The experimental equilibrium data were fitted very well with the Langmuir isotherm model, confirming the monolayer adsorption of CV onto adsorbent with a maximum monolayer adsorption capacity (q_{max}) of 39.64 mg g⁻¹ at 303 K. The value of Freundlich constant (n) and dimensionless separation factor (R_L) showed that the process was favorable. Thermodynamic parameters depicted the negative value of ΔG and the positive value of ΔH , confirmed that the process is spontaneous and endothermic in nature and, thus, the adsorption is favorable at higher temperatures. The value of ΔH and activation energy clearly revealed that the adsorption of CV onto adsorbent was a chemisorptive process. The kinetic experiments revealed that the adsorption process followed a pseudo-second-order rate equation. The overall rate of adsorption is controlled by both film and pore diffusion of dye molecules. It was found that external film diffusion controlled the dye uptake in the earlier stages, followed by pore diffusion, which controlled the rate at later stages. The Boyd and Bangham plots confirmed that the external film diffusion is the slowest step that mainly governs the rate of the reaction. Desorption studies on adsorbent showed that the maximum % of CV dye could be desorbed using the solvent ethanol. It shows that the % desorption decreased with the increase in the number of runs for all various desorbing reagents. The regenerated adsorbent can be used effectively up to three cycles to adsorb CV dye in aqueous solutions without any loss of adsorbent or appreciable reduction in adsorption efficiency. The experimental results showed that the NLP can be used as an excellent adsorbent for the removal of synthetic dye from wastewater. The better decolorization efficiency of CV, CR and mixture of other anionic dyes suggest that the NLP may be used effectively to decolorize anionic dyes from industrial effluents.

Symbols and abbreviations

A	—	Arrhenius frequency factor
AAD	—	Absolute average deviation
Adj MS	—	Adjusted mean squares
Adj SS	—	Adjusted sum of squares
AG	—	Acid green

ANOVA	— Analysis of variance	Seq SS	— Sequential sum of squares
ATR	— Attenuated transmission reflector	TGA	— Thermogravimetric analysis
BET	— Brunauer–Emmett–Teller	$T_{\text{statistics}}$	— Student 'T'-test
B_i	— Mathematical function of F	t	— Adsorption time, min
b_T	— Adsorption energy, kJ mole^{-1}	T	— Temperature, K
C	— Constant (Intercept value in intra-particle diffusion model), mg g^{-1}	V	— Volume of dye solution, mL
CCD	— Central composite design	W	— Mass of NLP adsorbent, g.
COD	— Chemical oxygen demand	x_i	— Dimensionless value of a process variable X_i
CR	— Congo red dye	X_i	— Real value of an independent variable
CV	— Coomassie violet dye	X_0	— Value of X_i at the center point
C_0	— Initial dye concentration in solution, mg L^{-1}	XRD	— X-ray diffraction
C_e	— Equilibrium dye concentration in solution, mg L^{-1}	X_1	— Initial pH
C_t	— Dye concentration in solution at any time t , mg L^{-1}	X_2	— Initial dye concentration, mg L^{-1}
DF	— Degree of freedom	X_3	— Adsorbent dosage, g
E_a	— Activation energy of adsorption, kJ mole^{-1}	X_4	— Agitation speed, rpm
EDAX	— Energy-dispersive X-ray spectroscopy	Y	— Predicted response variable, % color removal
F	— Ratio of amount of dye adsorbed at any time t to equilibrium	Y^p	— Actual response variable of % decolorization
$F_{\text{statistics}}$	— Fisher's 'F'-test	ΔG	— Changes in Gibbs free energy, kJ mole^{-1}
f	— Number of variables	ΔH	— Changes in enthalpy, kJ mole^{-1}
FESEM	— Field emission scanning electron microscopy	ΔS	— Changes in entropy, $\text{kJ mole}^{-1} \text{K}^{-1}$
h	— Initial rate of adsorption, $\text{mg g}^{-1} \text{min}^{-1}$	2^f	— Number of factorial points
K_a	— Adsorption equilibrium constant, L g^{-1}	2^f	— Axial points
K_F	— Freundlich isotherm constant, L g^{-1}	Greek letters	
K_i	— Intra-particle diffusion rate constant, $\text{mg g}^{-1} \text{min}^{-1/2}$	α	— Bangham model constant
K_L	— Langmuir isotherm constant, L mg^{-1}	β_0	— Offset term
K_T	— Temkin isotherm constant, L g^{-1}	β_i	— Regression coefficients for linear effect
K_1	— Pseudo-first-order rate constant, min^{-1}	β_{ii}	— Regression coefficients for quadratic effect
K_2	— Pseudo-second-order rate constant, $\text{g mg}^{-1} \text{min}^{-1}$	β_{ij}	— Regression coefficients for interaction effect
k_0	— Bangham model constant, $\text{L}^2 \text{g}^{-1}$	δX	— Step change
m	— Mass of adsorbent per volume of solution, g L^{-1}	χ^2	— Chi-square test value
N	— Numbers of experimental runs	References	
N_p	— Number of data points	[1]	J. Sahara, A. Naeema, M. Farooqa, S. Zareena, A.U. Rahman, Thermodynamic studies of adsorption of rhodamine B and Congo red on graphene oxide, <i>Desal. Water Treat.</i> , 164 (2019) 228–239.
N_0	— Number of center points	[2]	Y. Tang, M. Li, C. Mu, J. Zhou, B. Shi, Ultrafast and efficient removal of anionic dyes from wastewater by polyethyleneimine-modified silica nanoparticles, <i>Chemosphere</i> , 229 (2019) 570–579.
n	— Heterogeneity factor	[3]	P.S. Kumar, J. Pavithra, S. Suriya, M. Ramesh, K.A. Kumar, <i>Sargassum wightii</i> , a marine alga is the source for the production of algal oil, bio-oil, and application in the dye wastewater treatment, <i>Desal. Water Treat.</i> , 55 (2015) 1342–1358.
P	— Probability value	[4]	Y. Zhou, J. Lu, Y. Zhou, Y. Liu, Recent advances for dyes removal using novel adsorbents: a review, <i>Environ. Pollut.</i> , 252 (2019) 352–365.
PRESS	— Predicted residual sum of squares	[5]	V.S. Munagapati, D.S. Kim, Equilibrium isotherms, kinetics, and thermodynamics studies for Congo red adsorption using calcium alginate beads impregnated with nano-goethite, <i>Ecotoxicol. Environ. Saf.</i> , 141 (2017) 226–234.
q_e	— Amount of dye adsorbed at equilibrium, mg g^{-1}	[6]	A.R. Petcu, C.A. Lazar, E.A. Rogozea, N.L. Olteanu, A. Meghea, M. Mihaly, Nonionic microemulsion systems applied for removal of ionic dyes mixtures from textile industry wastewaters, <i>Sep. Purif. Technol.</i> , 158 (2016) 155–159.
$q_{e,\text{expt}}$	— Experimental adsorption capacity, mg g^{-1}	[7]	P. Vairavel, V.R. Murty, Continuous fixed-bed adsorption of Congo red dye by dual adsorbent (<i>Neurospora crassa</i> dead fungal biomass and wheat bran): experimental and theoretical breakthrough curves, immobilization and reusability studies, <i>Desal. Water Treat.</i> , 98 (2017) 276–293.
$q_{e,\text{calc}}$	— Calculated adsorption capacity, mg g^{-1}	[8]	S.N. Jain, P.R. Gogate, Adsorptive removal of acid violet 17 dye from wastewater using biosorbent obtained from NaOH and H_2SO_4 activation of fallen leaves of <i>Ficus racemosa</i> , <i>J. Mol. Liq.</i> , 243 (2017) 132–143.
q_{max}	— Theoretical monolayer maximum saturation capacity, mg g^{-1}		
q_t	— Amount of dye adsorbed on the adsorbent surface at any time t , min		
R	— Universal gas constant, $8.314 \text{ J mole}^{-1} \text{K}^{-1}$		
R^2	— Linear regression correlation coefficient		
R_L	— Langmuir isotherm separation factor		
RBBR	— Remazol brilliant blue-R		
RMSE	— Root mean square error		
RSM	— Response surface methodology		
S	— Value of S chart		
SD	— Standard deviation		
SE	— Standard error of coefficient		
SEM	— Scanning electron microscopy		

- [9] M. Naushad, Z.A. Allothman, M.R. Awual, S.M. Alfadul, T. Ahamad, Adsorption of rose Bengal dye from aqueous solution by amberlite Ira-938 resin: kinetics, isotherms, and thermodynamic studies, *Desal. Water Treat.*, 57 (2016) 13527–13533.
- [10] G. Sharma, M. Naushad, A. Kumar, S. Rana, S. Sharma, A. Bhatnagar, F.J. Stadler, A.A. Ghfar, M.R. Khan, Efficient removal of coomassie brilliant blue R-250 dye using starch/poly(alginate-chitosan) nanohydrogel, *Process Saf. Environ.*, 109 (2017) 301–310.
- [11] G. Sharma, M. Naushad, D. Pathania, A. Mittal, G.E. El-desoky, Modification of *Hibiscus cannabinus* fiber by graft copolymerization: application for dye removal, *Desal. Water Treat.*, 54 (2015) 3114–3121.
- [12] Z.A. Medvedev, H.M. Crowne, M.N. Medvedeva, Age related variations of hepatocarcinogenic effect of azo dye (3'-MDAB) as linked to the level of hepatocyte polyploidization, *Mech. Ageing Dev.*, 46 (1988) 159–174.
- [13] S.E. Subramani, D. Kumaresan, N. Thinakaran, Application of activated carbon derived from waste *Delonix regia* seed pods for the adsorption of acid dyes: kinetic and equilibrium studies, *Desal. Water Treat.*, 57 (2016) 7322–7333.
- [14] S. Dardouri, J. Sghaier, A comparative study of adsorption and regeneration with different agricultural wastes as adsorbents for the removal of methylene blue from aqueous solution, *Chin. J. Chem. Eng.*, 25 (2017) 1282–1287.
- [15] P. Vairavel, V.R. Murty, S. Nethaji, Removal of Congo red dye from aqueous solutions by adsorption onto a dual adsorbent (*Neurospora crassa* dead biomass and wheat bran): optimization, isotherm, and kinetics studies, *Desal. Water Treat.*, 68 (2017) 274–292.
- [16] A.B. Albadarin, M.N. Collins, M. Naushad, S. Shirazian, G. Walker, C. Mangwandi, Activated lignin-chitosan extruded blends for efficient adsorption of methylene blue, *Chem. Eng. J.*, 307 (2017) 264–272.
- [17] H. Singh, G. Chauhan, A.K. Jain, S.K. Sharma, Adsorptive potential of agricultural wastes for removal of dyes from aqueous solutions, *J. Environ. Chem. Eng.*, 5 (2017) 122–135.
- [18] W.X. Zhang, L. Lai, P. Mei, Y. Li, Y.H. Li, Y. Liu, Enhanced removal efficiency of acid red 18 from aqueous solution using wheat bran modified by multiple quaternary ammonium salts, *Chem. Phys. Lett.*, 710 (2018) 193–201.
- [19] Z.N. Garba, I. Bello, A. Galadima, A.Y. Lawal, Optimization of adsorption conditions using central composite design for the removal of copper(II) and lead(II) by defatted papaya seed, *Karbala Int. J. Mod. Sci.*, 2 (2016) 20–28.
- [20] A. Buthiyappan, J. Gopalan, A.A.A. Raman, Synthesis of iron oxides impregnated green adsorbent from sugarcane bagasse: characterization and evaluation of adsorption efficiency, *J. Environ. Manage.*, 249 (2019) 109323–109334.
- [21] K.M. Mousa, A.H. Taha, Adsorption of reactive blue dye onto natural and modified wheat straw, *J. Chem. Eng. Process Technol.*, 6 (2015) 260–265.
- [22] J.P. Fan, B. Zheng, Y. Qin, D. Yang, D.D. Liao, X.K. Xu, X.H. Zhang, J.H. Zhu, A superparamagnetic Fe₃O₄-graphene oxide nanocomposite for enrichment of nuciferine in the extract of *Nelumbinis folium* (Lotus leaf), *Appl. Surf. Sci.*, 364 (2016) 332–339.
- [23] R.K. Bharali, K.G. Bhattacharyya, Biosorption of fluoride on neem (*Azadirachta indica*) leaf powder, *J. Environ. Chem. Eng.*, 3 (2015) 662–669.
- [24] K.A. Adegoke, O.S. Bello, Dye sequestration using agricultural wastes as adsorbents, *Water Resour. Ind.*, 12 (2015) 8–24.
- [25] K.G. Bhattacharyya, A. Sharma, *Azadirachta indica* leaf powder as an effective biosorbent for dyes: a case study with aqueous Congo red solutions, *J. Environ. Manage.*, 71 (2004) 217–229.
- [26] M.A. Hossain, W.A.S. Al-Toubi, A.M. Weli, Q.A. Al-Riyami, J.N. Al-Sabahi, Identification and characterization of chemical compounds in different crude extracts from leaves of Omani neem, *J. Taibah Univ. Sci.*, 7 (2013) 181–188.
- [27] E. Vunain, D. Kenneth, T. Biswick, Synthesis and characterization of low-cost activated carbon prepared from Malawian baobab fruit shells by H₃PO₄ activation for removal of Cu(II) ions: equilibrium and kinetics studies, *Appl. Water Sci.*, 7 (2017) 4301–4319.
- [28] P. Vairavel, V.R. Murty, Optimization of batch process parameters for Congo red color removal by *Neurospora crassa* live fungal biomass with wheat bran dual adsorbent using response surface methodology, *Desal. Water Treat.*, 103 (2018) 84–101.
- [29] P. Vairavel, V.R. Murty, Optimization, kinetics, equilibrium isotherms and thermodynamics studies for Congo red dye adsorption using calcium alginate beads immobilized with dual adsorbent (*Neurospora crassa* dead fungal biomass and wheat bran), *Desal. Water Treat.*, 97 (2017) 338–362.
- [30] J. Maity, S.K. Ray, Removal of Pb(II) from water using a bio-composite adsorbent—a systematic approach of optimizing synthesis and process parameters by response surface methodology, *J. Environ. Manage.*, 209 (2018) 112–125.
- [31] B. Zhang, X. Han, P. Gu, S. Fang, J. Bai, Response surface methodology approach for optimization of ciprofloxacin adsorption using activated carbon derived from the residue of desiccated rice husk, *J. Mol. Liq.*, 238 (2017) 316–325.
- [32] A.S. Abdulhameed, A.K.T. Mohammad, A.H. Jawad, Modeling and mechanism of reactive orange 16 dye adsorption by chitosan-glyoxal/TiO₂ nanocomposite: application of response surface methodology, *Desal. Water Treat.*, 164 (2019) 346–360.
- [33] A.H. Jawad, N.S.A. Mubarak, S. Sabar, Adsorption and mechanism study for reactive red 120 dye removal by cross-linked chitosan-epichlorohydrin biobeads, *Desal. Water Treat.*, 164 (2019) 378–387.
- [34] H.M.F. Freundlich, Over the adsorption in solution, *J. Phys. Chem.*, 385 (1906) 385–470.
- [35] I. Langmuir, The adsorption of gases on plane surfaces of glass, mica and platinum, *J. Am. Chem. Soc.*, 40 (1918) 1361–1403.
- [36] K.R. Hall, L.C. Eagleton, A. Acrivos, T. Vermeulen, Pore and solid diffusion kinetics in fixed-bed adsorption under constant pattern conditions, *Ind. Eng. Chem. Fundam.*, 5 (1966) 212–223.
- [37] L. Mouni, L. Belkhir, J.C. Bollinger, A. Bouzaza, A. Assadi, A. Tirri, F. Dahmoune, K. Madani, H. Remini, Removal of methylene blue from aqueous solutions by adsorption on Kaolin: kinetic and equilibrium studies, *Appl. Clay Sci.*, 153 (2018) 38–45.
- [38] M.J. Temkin, V. Pyzhev, Kinetics of ammonia synthesis on promoted iron catalysts, *Acta Phys. Chim.*, 12 (1940) 217–222.
- [39] V.S. Munagapati, D.S. Kim, Adsorption of anionic azo dye congo red from aqueous solution by cationic modified orange peel powder, *J. Mol. Liq.*, 220 (2016) 540–548.
- [40] A.A. Alqadami, M. Naushad, M.A. Abdalla, M.R. Khan, Z.A. Allothman, Adsorptive removal of toxic dye using Fe₃O₄-TSC nanocomposite: equilibrium, kinetic, and thermodynamic studies, *J. Chem. Eng. Data*, 61 (2016) 3806–3813.
- [41] D. Garg, C.B. Majumder, S. Kumar, B. Sarkar, Removal of direct blue-86 dye from aqueous solution using alginate encapsulated activated carbon (PnsAC-alginate) prepared from waste peanut shell, *J. Environ. Chem. Eng.*, 7 (2019) 103365–103378.
- [42] V.K. Gupta, D. Pathania, S. Sharma, S. Agarwal, P. Singh, Remediation and recovery of methyl orange from aqueous solution onto acrylic acid grafted *Ficus carica* fiber: isotherms, kinetics and thermodynamics, *J. Mol. Liq.*, 177 (2013) 325–334.
- [43] A.A. Alqadami, M. Naushad, Z.A. Allothman, A.A. Ghfar, Novel metal-organic framework (MOF) based composite material for the sequestration of U(VI) and Th(IV) metal ions from aqueous environment, *ACS Appl. Mater. Interfaces*, 9 (2017) 36026–36037.
- [44] T. Tatarchuk, N. Paliychuk, R.B. Bitra, A. Shyichuk, M. Naushad, I. Mironyuk, D. Ziolkowska, Adsorptive removal of toxic methylene blue and Acid Orange 7 dyes from aqueous medium using cobalt-zinc ferrite nanoadsorbents, *Desal. Water Treat.*, 150 (2019) 374–385.
- [45] M. Makrygianni, Z.G. Lada, A. Manousou, C.A. Aggelopoulos, V. Deimede, Removal of anionic dyes from aqueous solution by novel pyrrolidinium-based polymeric ionic liquid (PIL) as adsorbent: investigation of the adsorption kinetics, equilibrium isotherms and the adsorption mechanisms involved, *J. Environ. Chem. Eng.*, 7 (2019) 103163–103173.

- [46] J.P. Calderon, M.V. Santos, N. Zaritzky, Reactive RED 195 dye removal using chitosan coacervated particles as bio-sorbent: analysis of kinetics, equilibrium and adsorption mechanisms, *J. Environ. Chem. Eng.*, 6 (2018) 6749–6760.
- [47] S. Lagergren, Zur theorie der sogenannten adsorption gelöster stoffe, *Kungliga svenska vetenskapsakademiens, Handlingar*, 24 (1898) 1–39.
- [48] Y.S. Ho, G. McKay, Pseudo-second-order model for sorption processes, *Process Biochem.*, 34 (1999) 451–465.
- [49] S. Shakoor, A. Nasar, Removal of methylene blue dye from artificially contaminated water using *Citrus limetta* peel waste as a very low cost adsorbent, *J. Taiwan Inst. Chem. Eng.*, 66 (2016) 154–163.
- [50] D. Pathania, A. Sharma, Z.M. Siddiqi, Removal of Congo red dye from aqueous system using *Phoenix dactylifera* seeds, *J. Mol. Liq.*, 219 (2016) 359–367.
- [51] P. Terangpi, S. Chakraborty, Adsorption kinetics and equilibrium studies for removal of acid azo dyes by aniline formaldehyde condensate, *Appl. Water Sci.*, 7 (2017) 3661–3671.
- [52] D.D. Sewu, P. Boakye, S.H. Woo, Highly efficient adsorption of cationic dye by biochar produced with Korean cabbage waste, *Bioresour. Technol.*, 224 (2017) 206–213.
- [53] E. Daneshvar, A. Vazirzadeh, A. Niazi, M. Kousha, M. Naushad, A. Bhatnagar, Desorption of methylene blue dye from brown macroalgae: effects of operating parameters, isotherm study and kinetic modeling, *J. Cleaner Prod.*, 152 (2017) 443–453.
- [54] O.A. Ekpete, A.C. Marcus, V. Osi, Preparation and characterization of activated carbon obtained from plantain (*Musa paradisiaca*) fruit stem, *J. Chem.*, 2017 (2017) 1–6.
- [55] M. Rajib, C.T. Oguchi, S.M.M. Hasan, In-situ oxidation effect on pore size distribution in investigating adsorption properties under various geochemical conditions, *Solid Earth Sci.*, 4 (2019) 113–124.
- [56] P.C. Jain, M. Jain, *Engineering Chemistry (Chemistry of Engineering Materials)*, 9th ed., Dhanpat Rai & Sons Publishing Company Ltd., India, 1992.
- [57] B.H. Stuart, *Infrared Spectroscopy: Fundamentals and Applications*, John Wiley & Sons Ltd., New York, USA, 2004.
- [58] L. Gnanasekaran, R. Hemamalini, M. Naushad, Efficient photocatalytic degradation of toxic dyes using nanostructured TiO₂/polyaniline nanocomposite, *Desal. Water Treat.*, 108 (2018) 322–328.
- [59] S. Salla, N.R. Ankem, P.S. Kumar, A.A. Renita, K. Micheal, Enhanced photocatalytic activity of environment-friendly C/ZnFe₂O₄ nanocomposites: application in dye removal, *Desal. Water Treat.*, 137 (2019) 395–402.
- [60] R.M. Ali, H.A. Hamad, M.M. Hussein, G.F. Malash, Potential of using green adsorbent of heavy metal removal from aqueous solutions: adsorption kinetics, isotherm, thermodynamic, mechanism and economic analysis, *Ecol. Eng.*, 91 (2016) 317–332.
- [61] D. Montgomery, G.C. Runger, *Applied statistics and probability for engineers*, 5th ed., John Wiley & Sons Ltd., New York, USA, 2011.
- [62] A. Takdastan, S. Samarbaef, Y. Tahmasebi, N. Alavi, A.A. Babaei, Alkali modified oak waste residues as a cost-effective adsorbent for enhanced removal of cadmium from water: isotherm, kinetic, thermodynamic and artificial neural network modeling, *J. Ind. Eng. Chem.*, 78 (2019) 352–363.
- [63] N. Kannan, S. Murugavel, Comparative study on the removal of acid violet by adsorption on various low cost adsorbents, *Global NEST J.*, 10 (2008) 395–403.
- [64] M.R. Patil, V.S. Shrivastava, Adsorption removal of carcinogenic acid violet19 dye from aqueous solution by polyaniline-Fe₂O₃ magnetic nano-composite, *J. Mater. Environ. Sci.*, 6 (2015) 11–21.
- [65] C. Namasivayam, R.T. Yamuna, D.J.S.E. Arasi, Removal of acid violet from waste water by adsorption on waste red mud, *Environ. Geol.*, 41 (2001) 269–273.
- [66] O. Anjaneya, M. Santoshkumar, S.N. Anand, T.B. Karegoudar, Biosorption of acid violet dye from aqueous solutions using native biomass of a new isolate of *Penicillium* sp., *Int. Biodeterior. Biodegrad.*, 63 (2009) 782–787.
- [67] D. Edison, K.S. Ramesh, M.S. Sivaramkumar, R. Velmurugan, Removal of acid violet 19 dye from aqueous solution by adsorption onto activated charcoal and polyaniline coated charcoal, *Int. J. Trend Res. Dev.*, 3 (2016) 22–27.
- [68] C. Namasivayam, R. Radhika, S. Suba, Uptake of dyes by a promising locally available agricultural solid waste: coir pith, *Waste Manage.*, 21 (2001) 381–387.
- [69] C. Namasivayam, N. Kanchana, Waste banana pith as adsorbent for color removal from wastewaters, *Chemosphere*, 25 (1992) 1691–1705.
- [70] S. Rajeshwari, C. Namasivayam, K. Kadirvelu, Orange peel as an adsorbent in the removal of acid violet 17 (acid dye) from aqueous solutions, *Waste Manage.*, 21 (2001) 105–110.
- [71] Sumanjit, T.P.S. Walia, R. Kaur, Removal of health hazards causing acidic dyes from aqueous solutions by the process of adsorption, *Online J. Health Allied Sci.*, 3 (2007) 1–10.
- [72] W. Konicki, A. Helminiak, W. Arabczyk, E. Mijowska, Removal of anionic dyes using magnetic Fe@graphite core-shell nanocomposite as an adsorbent from aqueous solutions, *J. Colloid Interface Sci.*, 497 (2017) 155–164.
- [73] H. Shayesteh, A.R. Kelishami, R. Norouzbeigi, Evaluation of natural and cationic surfactant modified pumice for Congo red removal in batch mode: kinetic, equilibrium, and thermodynamic studies, *J. Mol. Liq.*, 221 (2016) 1–11.
- [74] R.A. Reza, M. Ahmaruzzaman, A novel synthesis of Fe₂O₃@activated carbon composite and its exploitation for the elimination of carcinogenic textile dye from an aqueous phase, *RSC Adv.*, 5 (2015) 10575–10586.
- [75] R. Sahraei, K. Hemmati, M. Ghaemy, Adsorptive removal of toxic metals and cationic dyes by magnetic adsorbent based on functionalized graphene oxide from water, *RSC Adv.*, 76 (2016) 72487–72499.

Supplementary information:

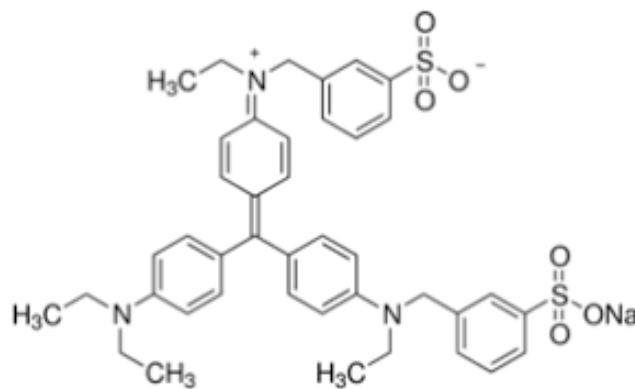


Fig. S1. Molecular structure of Coomassie violet dye.

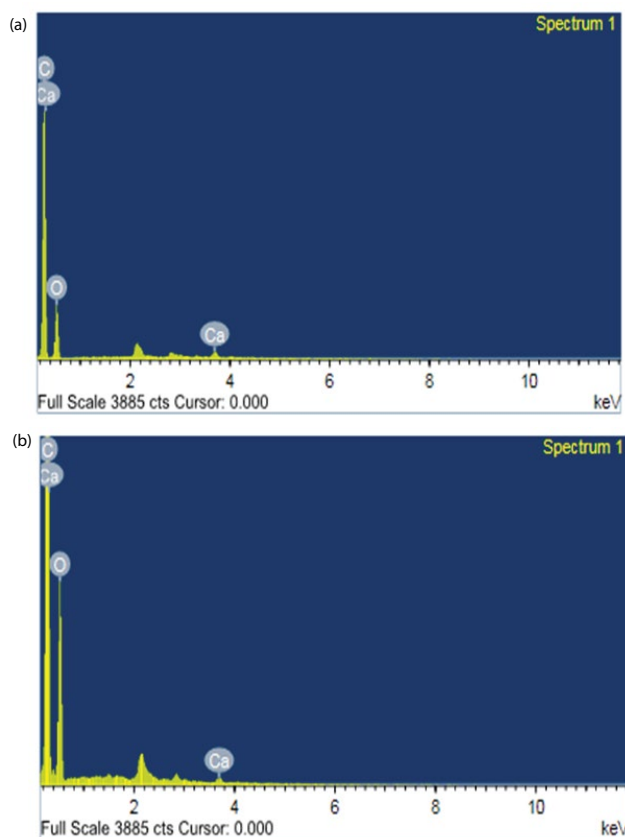


Fig. S2. (a) EDAX analysis of neem leaf fine powder (NLP) adsorbent before CV dye adsorption and (b) EDAX analysis of NLP adsorbent after CV dye adsorption.

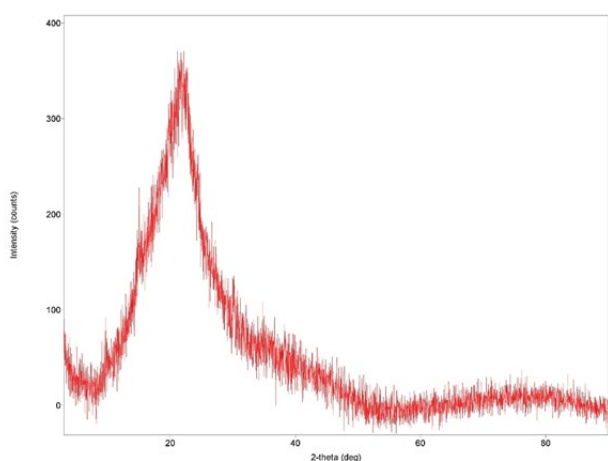


Fig. S3. XRD analysis of NLP adsorbent before CV dye adsorption.

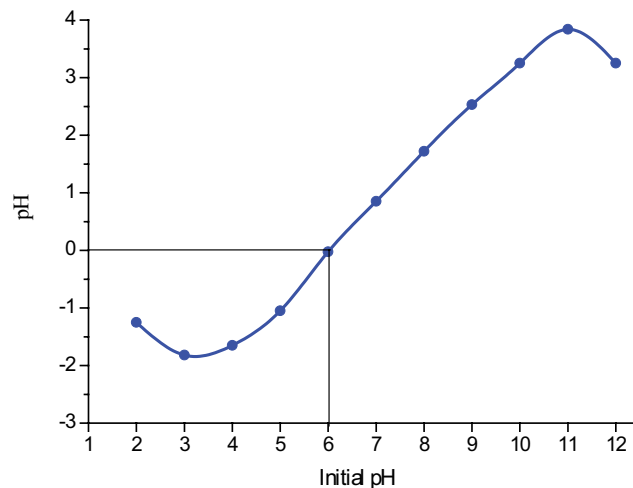


Fig. S4. Zero-point charge (pH_{zpc}) plot of prepared NLP adsorbent. (Sodium chloride concentration: 0.01 M; adsorbent dosage: 5 g L⁻¹; agitation speed: 150 rpm; temperature: 303 K; contact time 48 h).

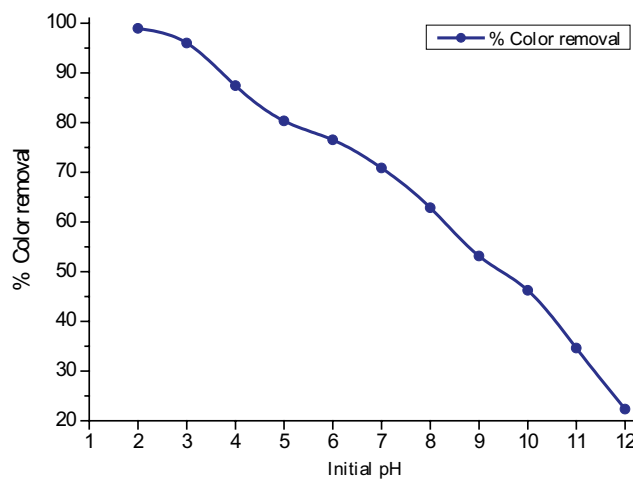


Fig. S5. Effect of initial pH on the removal of CV dye by NLP adsorbent. (Initial dye concentration: 100 mg L⁻¹; adsorbent dosage: 5 g L⁻¹; adsorbent particle size: 125 μm; agitation speed: 180 rpm; temperature: 303 K; contact time: 6 h).

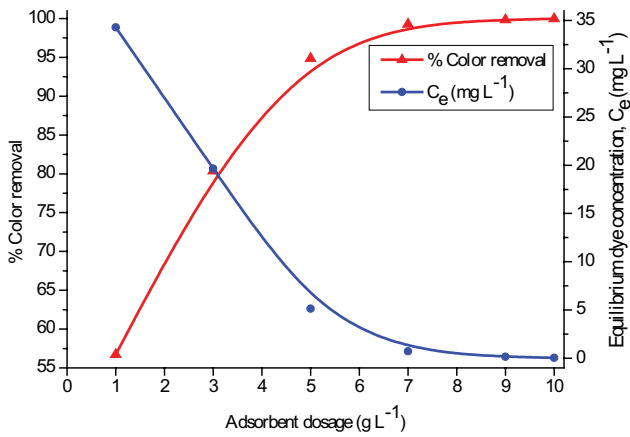


Fig. S6. Effect of NLP adsorbent dosage on CV dye adsorption. (Initial pH: 2; initial dye concentration: 100 mg L⁻¹; adsorbent particle size: 125 μm; agitation speed: 180 rpm; temperature: 303 K; contact time: 24 h).

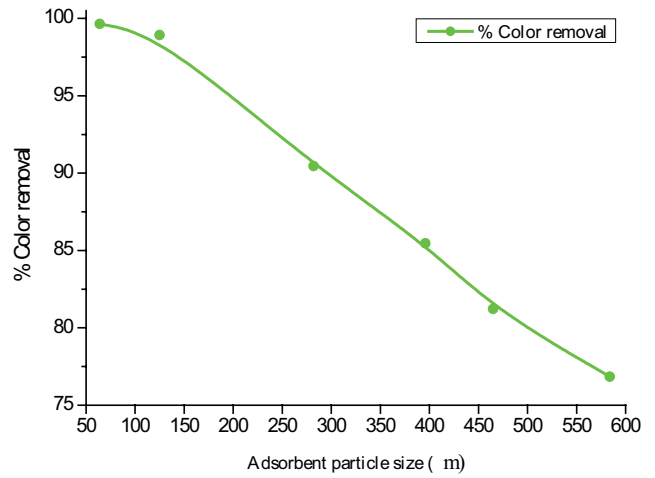


Fig. S7. Effect of NLP adsorbent particle size on CV dye adsorption. (Initial pH: 2; initial dye concentration: 100 mg L⁻¹; adsorbent dosage: 5 g L⁻¹; agitation speed: 180 rpm; temperature: 303 K; contact time: 6 h).

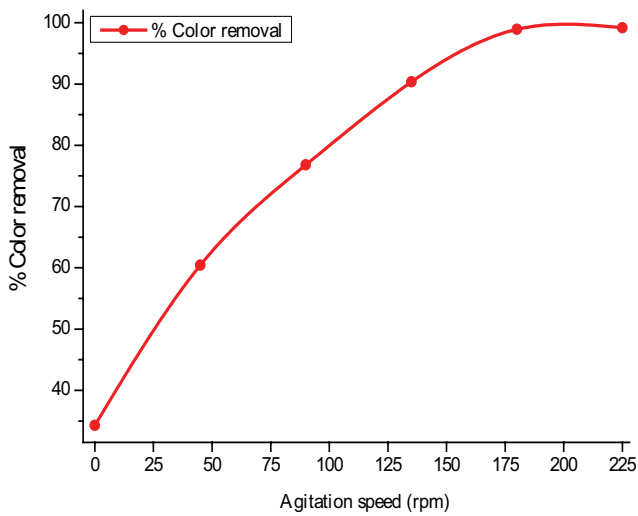


Fig. S8. Effect of agitation speed on the removal of CV by NL adsorbent. (Initial pH: 6; initial dye concentration: 100 mg L⁻¹; adsorbent dosage: 5 g L⁻¹; adsorbent particle size: 125 μm; temperature: 303 K; contact time: 6 h).

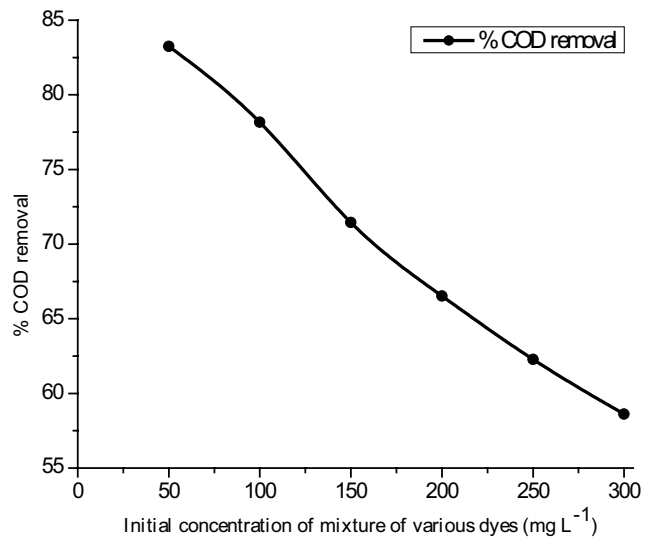


Fig. S9. Effect of initial dye concentration on a mixture of dyes by NLP adsorbent. (Initial pH: 2; initial dye concentration: 50–300 mg L⁻¹; adsorbent dosage: 6 g L⁻¹; adsorbent particle size: 125 μm; agitation speed: 180 rpm; temperature: 303 K; contact time: 6 h).

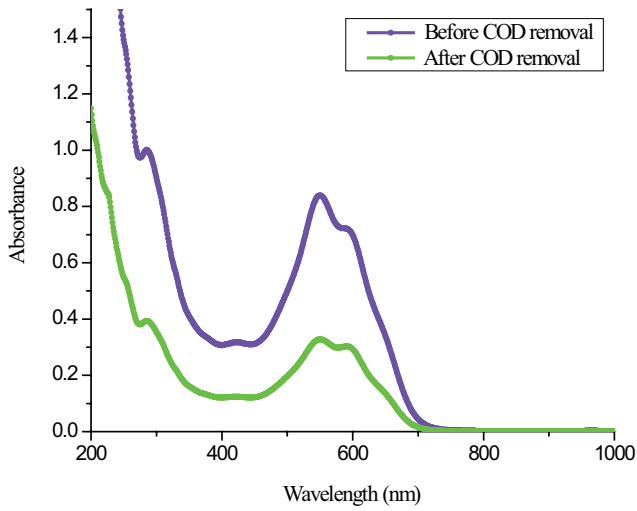


Fig. S10. Profile of synthetic dye effluent mixture before and after COD removal, (Initial pH: 2; initial dye concentration: 100 mg L⁻¹; adsorbent dosage: 6 g L⁻¹; adsorbent particle size: 125 μm; agitation speed: 180 rpm; temperature: 303 K; contact time: 6 h).

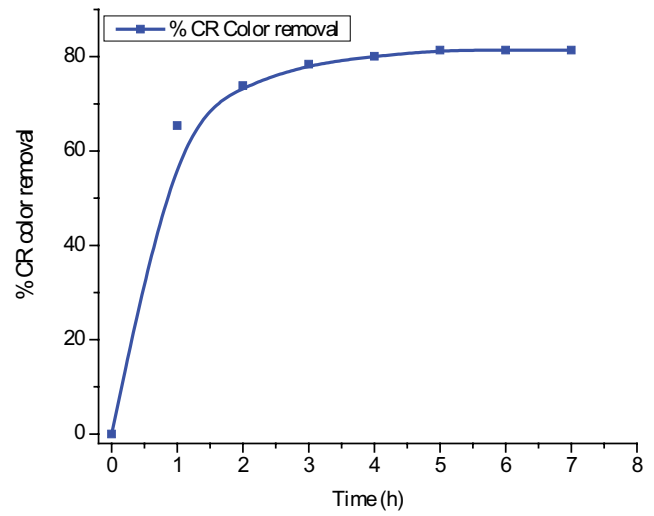


Fig. S11. Effect of time on the removal of CR dye by NLP adsorbent. (Initial pH: 6; initial dye concentration: 200 mg L⁻¹; adsorbent dosage: 6 g L⁻¹; adsorbent particle size: 125 μm; agitation speed: 180 rpm; temperature: 303 K; contact time: 6 h).

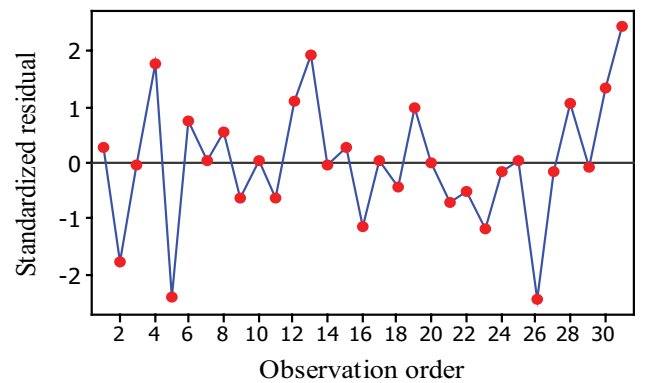
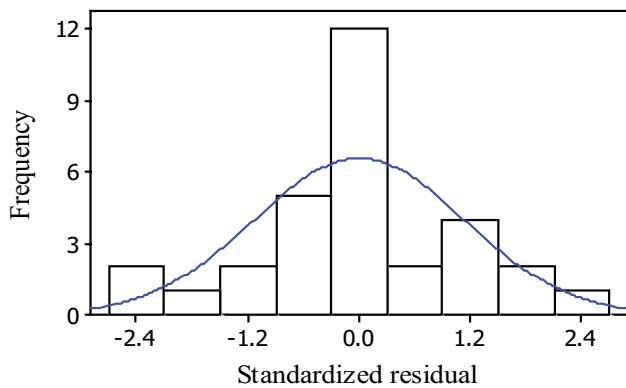
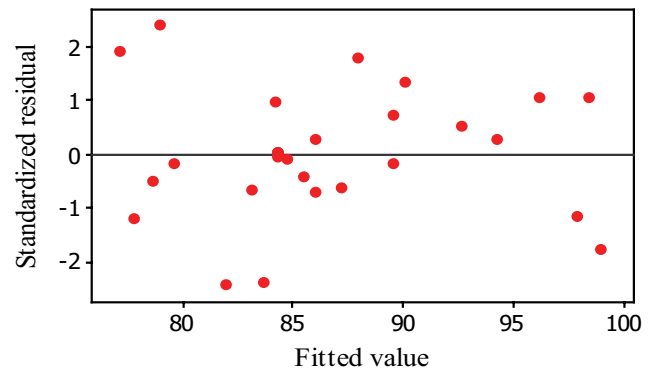
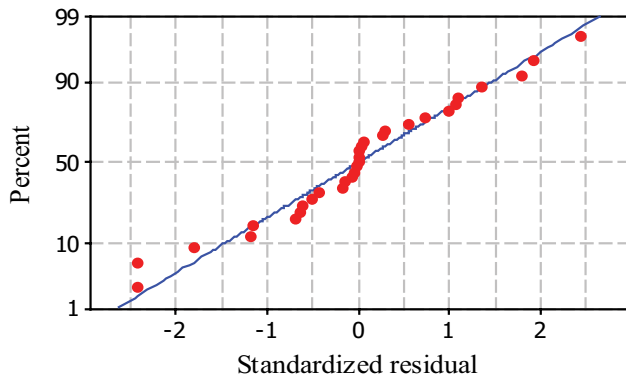


Fig. S12. Residual plots for CV color removal by NLP adsorbent. (a) Normal probability plot of standardized residuals, (b) Standardized residuals vs. fitted values, (c) Frequency of observation vs. standardized residuals, and (d) Standardized residuals vs. the order of the data.

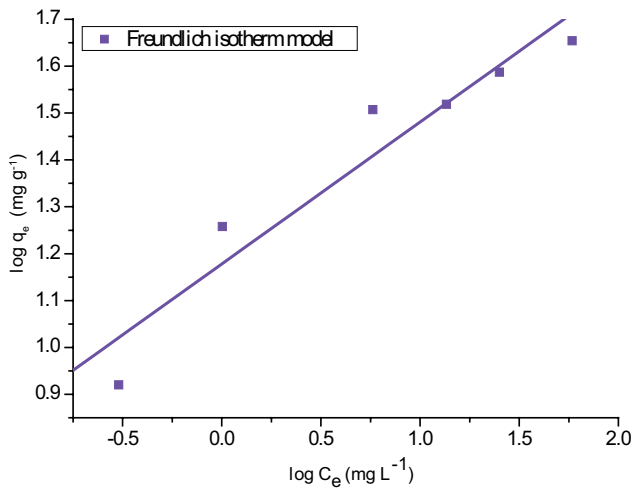


Fig. S13. Freundlich isotherm plot for adsorption of CV dye onto NLP adsorbent. (Initial pH: 2; initial dye concentration: 50–300 mg L⁻¹; adsorbent dosage: 6 g L⁻¹; adsorbent particle size: 125 μm; agitation speed: 180 rpm; temperature: 303 K; contact time: 24 h).

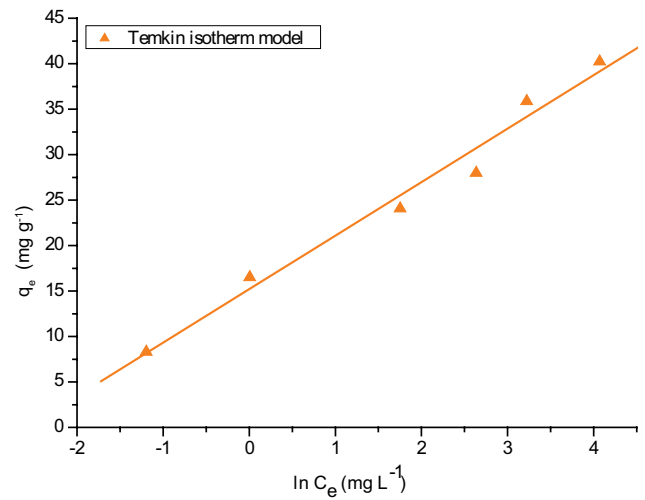


Fig. S14. Temkin isotherm plot for adsorption of CV dye onto NLP adsorbent. (Initial pH: 2; initial dye concentration: 50–300 mg L⁻¹; adsorbent dosage: 6 g L⁻¹; adsorbent particle size: 125 μm; agitation speed: 180 rpm; temperature: 303 K; contact time: 24 h).

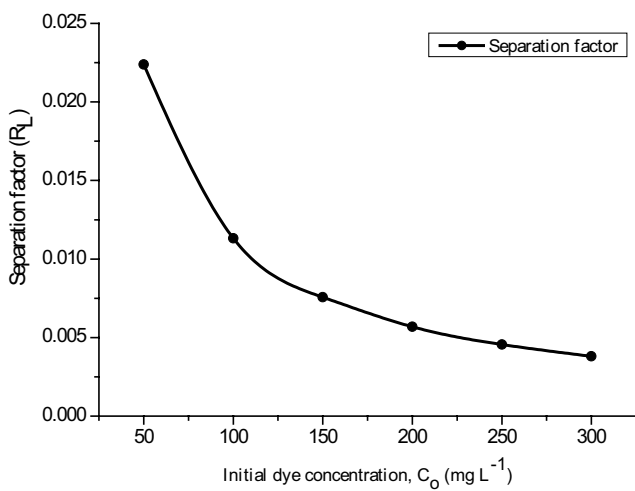


Fig. S15. Separation factor for adsorption of CV dye onto NLP adsorbent. (Initial pH: 2; CV dye concentration: 50–300 mg L⁻¹; adsorbent dosage: 6 g L⁻¹; adsorbent particle size: 125 μm; agitation speed: 180 rpm; temperature: 303 K; contact time: 24 h).

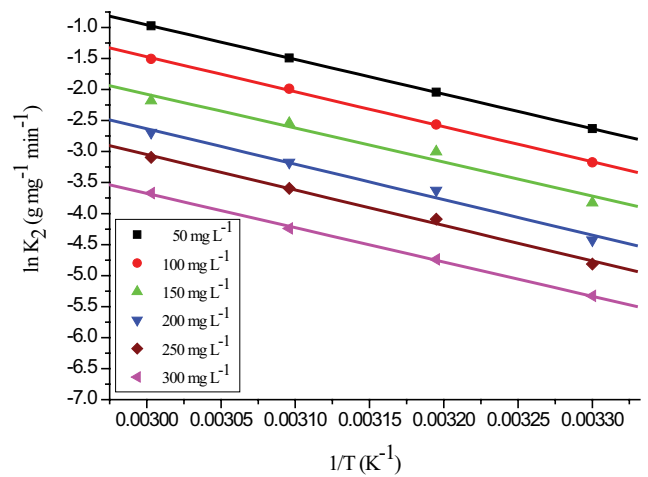


Fig. S16. Arrhenius plot for adsorption of CV dye onto NLP adsorbent. (Initial pH: 2; initial dye concentration: 50–300 mg L⁻¹; adsorbent dosage: 6 g L⁻¹; adsorbent particle size: 125 μm; agitation speed: 180 rpm; contact time: 24 h).

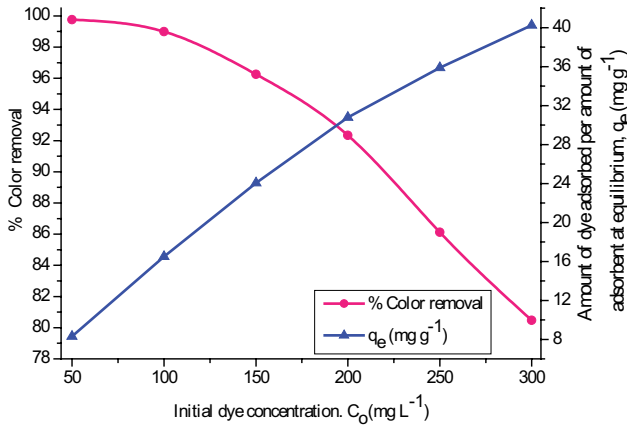


Fig. S17. Effect of initial dye concentration on the removal of CV dye by NLP adsorbent. (Initial pH: 2; adsorbent dosage: 6 g L⁻¹; adsorbent particle size: 125 μm; agitation speed: 180 rpm; temperature: 303 K; contact time: 24 h).

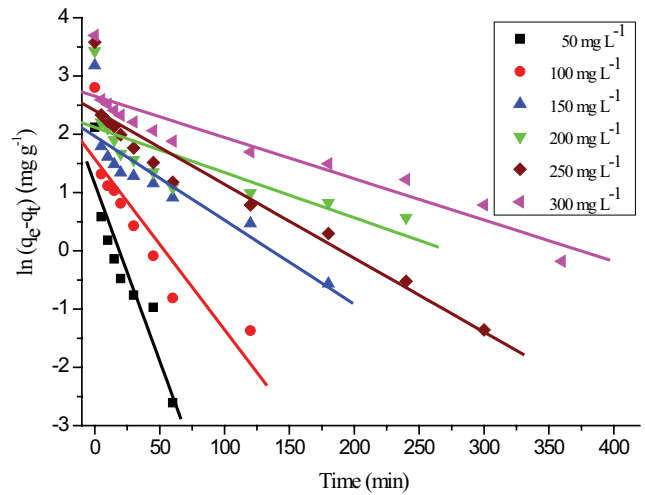


Fig. S18. Lagergren pseudo-first-order kinetic plot for adsorption of CV dye onto NLP adsorbent. (Initial pH: 2; initial dye concentration: 50–300 mg L⁻¹; adsorbent dosage: 6 g L⁻¹; adsorbent particle size: 125 μm; agitation speed: 180 rpm; temperature: 303 K; contact time: 24 h).

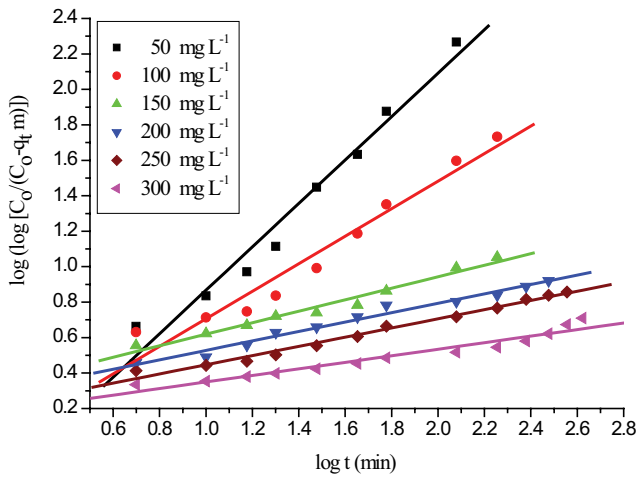


Fig. S19. Bangham plot for adsorption of CV dye onto NLP adsorbent. (Initial pH: 2; initial dye concentration: 50–300 mg L⁻¹; adsorbent dosage: 6 g L⁻¹; adsorbent particle size: 125 μm; agitation speed: 180 rpm; temperature: 303 K; contact time: 24 h).

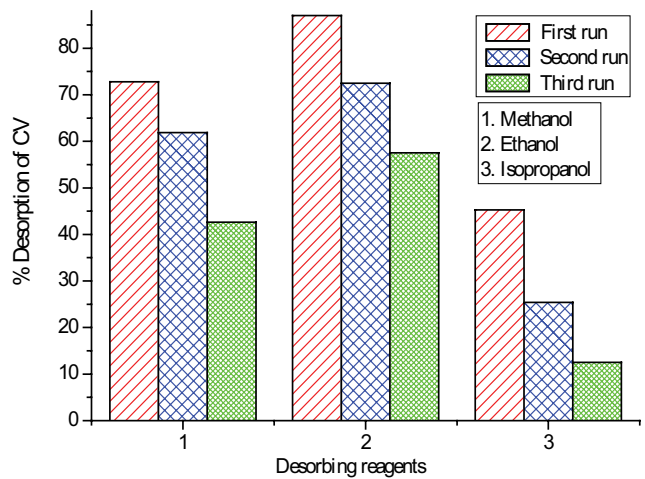


Fig. S20. Desorption efficiency of CV from NLP adsorbent in various runs. (Volume of desorbing reagent: 100 mL; shaking speed: 180 rpm; temperature: 303 K; contact time: 24 h).

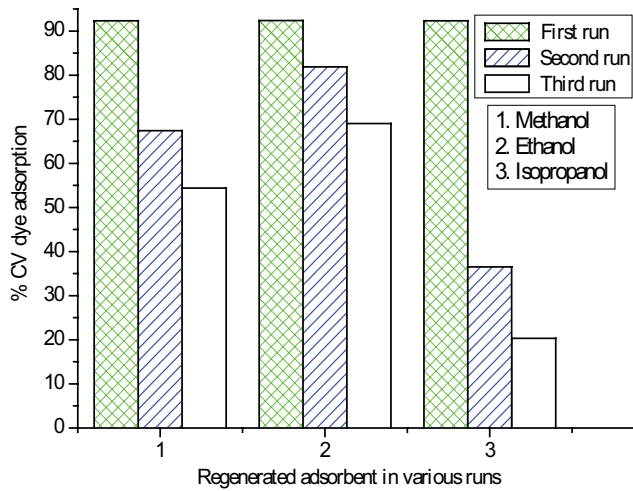


Fig. S21. Reusability of NLP adsorbent for the adsorption of CV dye in various runs. (Initial pH: 2; initial dye concentration: 200 mg L⁻¹; volume of dye solution: 100 mL; agitation speed: 180 rpm; temperature: 303 K; contact time: 24 h).

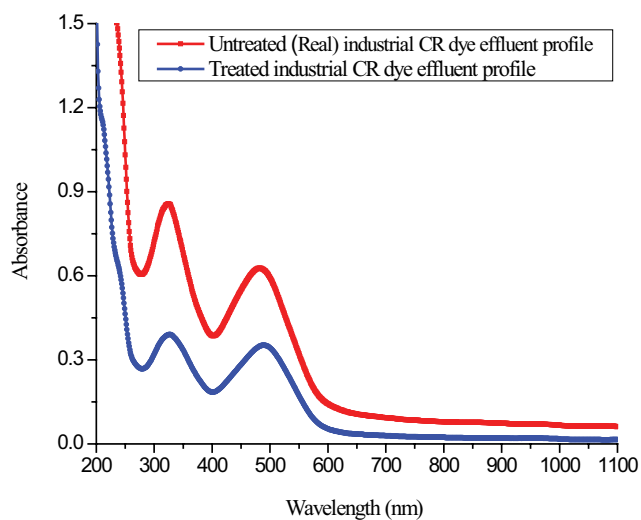


Fig. S22. Industrial CR dye effluent adsorption profile obtained in batch studies using NLP adsorbent with an untreated effluent profile. (Initial pH: 8.5; initial COD: 1,824 mg L⁻¹; initial adsorbate concentration: 200 mg L⁻¹; adsorbent dosage: 6 g L⁻¹; adsorbent particle size: 125 μm; agitation speed: 180 rpm; temperature: 303 K; contact time: 24 h).

Table S1
Physical properties of NLP adsorbent

Parameters	Values (%)
Moisture content	6.94
Volatile matter	54.36
Ash content	8.92
Fixed carbon	29.78

Table S2
Activation energy for the adsorption of CV dye onto NLP adsorbent at various initial dye concentrations

Initial dye concentration (mg L ⁻¹)	Activation energy, E _a (kJ mole ⁻¹)
50	46.408
100	46.922
150	45.561
200	47.549
250	47.512
300	45.963

Table S3
Desorption studies for the removal of CV dye from NLP adsorbent in various runs

Sl. No	Desorbing agent	% desorption of CV dye from the NL adsorbent		
		1 st run	2 nd run	3 rd run
1	Methanol	72.80	61.86	42.63
2	Ethanol	87.02	72.46	57.53
3	Isopropanol	45.26	25.38	12.54

Table S4
Reusability of NLP adsorbent for the adsorption of CV dye in various runs

Sl. No	Desorbing agent	% adsorption of CV dye by regenerated NL adsorbent		
		1 st run	2 nd run	3 rd run
1	Methanol	92.34	67.42	54.38
2	Ethanol	92.36	81.86	69.02
3	Isopropanol	92.33	36.53	20.31